

Intrinsic fractional noise in nanopores: The effect of reservoirs

Cite as: J. Chem. Phys. **154**, 171101 (2021); <https://doi.org/10.1063/5.0047380>

Submitted: 12 February 2021 . Accepted: 09 April 2021 . Published Online: 03 May 2021

 S. Marbach

COLLECTIONS

Paper published as part of the special topic on [Fluids in Nanopores](#)



View Online



Export Citation



CrossMark

ARTICLES YOU MAY BE INTERESTED IN

[Bursting the bubble: A molecular understanding of surfactant-water interfaces](#)

The Journal of Chemical Physics **154**, 170901 (2021); <https://doi.org/10.1063/5.0047377>

[Resetting transition is governed by an interplay between thermal and potential energy](#)

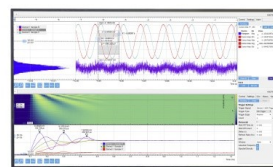
The Journal of Chemical Physics **154**, 171103 (2021); <https://doi.org/10.1063/5.0049642>

[Extended magnesium and calcium force field parameters for accurate ion-nucleic acid interactions in biomolecular simulations](#)

The Journal of Chemical Physics **154**, 171102 (2021); <https://doi.org/10.1063/5.0048113>

Challenge us.

What are your needs for
periodic signal detection?



Zurich
Instruments

Intrinsic fractional noise in nanopores: The effect of reservoirs

Cite as: J. Chem. Phys. 154, 171101 (2021); doi: 10.1063/5.0047380

Submitted: 12 February 2021 • Accepted: 9 April 2021 •

Published Online: 3 May 2021



View Online



Export Citation



CrossMark

S. Marbach^{a)} 

AFFILIATIONS

Courant Institute for Mathematical Sciences, New York University, New York, 10012, USA and CNRS, Sorbonne Université, Physicochimie des Electrolytes et Nanosystèmes Interfaciaux, F-75005 Paris, France

Note: This paper is part of the JCP Special Topic on Fluids in Nanopores.

^{a)} Author to whom correspondence should be addressed: sophie@marbach.fr

ABSTRACT

Fluctuations affect nanoporous transport in complex and intricate ways, making optimization of the signal-to-noise ratio in artificial designs challenging. Here, we focus on the simplest nanopore system, where non-interacting particles diffuse through a pore separating reservoirs. We find that the concentration difference between both sides (akin to the osmotic pressure drop) exhibits fractional noise in time t with mean square average that grows as $t^{1/2}$. This originates from the diffusive exchange of particles from one region to another. We fully rationalize this effect, with particle simulations and analytic solutions. We further infer the parameters (pore radius and pore thickness) that control this exotic behavior. As a consequence, we show that the number of particles *within* the pore also exhibits fractional noise. Such fractional noise is responsible for noise spectral density scaling as $1/f^{3/2}$ with frequency f , and we quantify its amplitude. Our theoretical approach is applicable to more complex nanoporous systems (for example, with adsorption within the pore) and drastically simplifies both particle simulations and analytic calculus.

Published under license by AIP Publishing. <https://doi.org/10.1063/5.0047380>

I. INTRODUCTION

A. General introduction

Fluctuations are ubiquitous in biological and artificial nanopores. The nanopore structure,^{1–3} its position on the membrane,⁴ its inner physical properties such as the local surface charge,⁵ and finally the number of particles inside and outside of the pore are all inherent sources of fluctuations. Their consequences on nanoporous transport are intricate and leave, in particular, strong signatures in noise measurements of currents. For example, the fluctuations of ionic current through a nanopore usually exhibit strong frequency dependence at low frequencies. Typically, the power spectral density of the current scales as $S(f) \sim 1/f^\alpha$, where $\alpha = 0.5–2.0$ according to the specifics of the system. Such a power law dependence, generally referred to as *low frequency noise*, has been measured repeatedly in biological pores^{1,2,6,7} and in a great diversity of artificial nanopores.^{2,8–19}

Understanding precisely the origin and magnitude of such noise is important for two reasons: First, to shed light on the transport mechanism and allow us to track single molecule events.^{20–22}

Second, to provide guidelines to optimize the signal-to-noise ratio to improve sensitivity of single molecule detection experiments or DNA sequencing.^{23–26} Most efforts on improving the signal-to-noise ratio are experimental and have been directed toward developing multilayered,^{27–29} surface treated pores to improve insulation^{30,31} or adsorption effects.³² Yet, theoretical advances are necessary to open new optimization avenues and improve our general understanding of noise in nanoporous transport.

First-principles theories for fluctuations in nanoscale systems have remained sparse as theoretical treatments face several challenges, such as solving equations in complex geometries^{33–35} or accounting for all the various interactions between solute particles.^{36,37} Furthermore, noise on ionic currents does not result from a single effect but from a combination of various effects that are more or less important according to the system investigated.¹⁴ Recent modeling advances have, nonetheless, pointed to the crucial role of adsorption inside the pores,^{32,35} of ion–ion correlations,³⁷ and of ionic concentration.³⁶ Most importantly, quantification of the amplitude of different noise sources is seldom available.

Here, we come back to basics and explore the simplest possible setting for nanoporous transport, with a focus on reservoir effects. We study non-interacting solute particles diffusing between two compartments separated by a membrane with a single pore—see Figs. 1(a) and 1(b). We investigate relevant observables in this context: (i) the concentration difference ΔN between the two compartments (akin to the osmotic pressure drop at small concentration differences³⁸), (ii) the current of (uncharged) particles crossing the membrane, and (iii) the number of particles within the pore. We find that such a simple system features very non-trivial noise characteristics. For example, fluctuations of the concentration difference grow as a power law $\langle \Delta N^2(t) \rangle \sim t^p$ (and reach a plateau at long times). The power law factor $p = 0.5-1$ according to the radius of the pore—see Fig. 1(c). Notably, this results in a noise spectrum $S(\Delta N, f) \sim 1/f^{1+p}$ —see Fig. 1(d). We will show that similar power law dependencies are seen in the other observables (ii) and (iii). Importantly, such fractional noise (with $p = 0.5$) is reminiscent of an intrinsic mathematical property of Brownian walkers exchanging between two sides of an imaginary boundary on a line.^{39,40} Its consequences in the context of nanoporous transport have yet to be observed and rationalized. Interestingly, such power law dependencies have been repeatedly observed in experimental or theoretical observations albeit rarely explained.^{1,2,17,52,35}

In this paper, we fully rationalize, theoretically and numerically, the emergence of fractional noise in these observables (i)–(iii). Our numerical model is based on Brownian dynamics of non-interacting, uncharged, particles. Our analytic treatment relies on a mapping of the full 3D problem to a simpler 1D problem, preserving equilibrium properties. This allows us to bypass geometric complexities^{34,35} and obtain analytic expressions. We show that the mapping solutions reproduce exactly Brownian dynamics simulations in 3D.

It further builds a general numerical framework to account efficiently for the effect of reservoirs without the introduction of artificial pore entry rates.⁴¹ Our analytic results shed light on the mechanisms at play. Interestingly, we find that $1/f^{3/2}$ noise spectra are predominantly seen in thick pores (akin to channels), while $1/f^2$ spectra correspond to thin pores. We further find a $1/f^{1/2}$ low frequency decay for the number of particles within the pore. Importantly, we are able to quantify their amplitude in terms of the parameters of the system (pore size and pore thickness). From these results, we deduce rules to optimize the signal-to-noise ratio in several cases. In particular, for currents associated with the number of particles within the pore (akin to the number of charge carriers for charged species), we find that the signal-to-noise ratio is maximized for *short* pores (in contrast with long pores).

B. Setup to probe the effect of reservoirs

In this study, we consider a simple nanoporous system, where particles—representing the solute species—may diffuse freely across a membrane pore of characteristic width R set on a membrane square of size $2L_m \times 2L_m$ —see Figs. 1(a) and 1(b). In Fig. 1(a), the pore is a circular pore of radius R . The radius R corresponds to the accessible pore radius. Our derivation is not limited to circular pores and can be easily extended to other cross sections such as slits. Let x be the direction orthogonal to the membrane plane and y and z along it. $x = y = z = 0$ corresponds to the position of the pore center on the membrane. We consider periodic boundary conditions in y and z at distance L_m from the pore center [dashed lines in Fig. 1(b)]. This means that the open area with respect to the total area of the membrane is $\pi R^2/4L_m^2$. When $R \sim L_m$, this corresponds to a large pore (or, making use of the periodic boundary

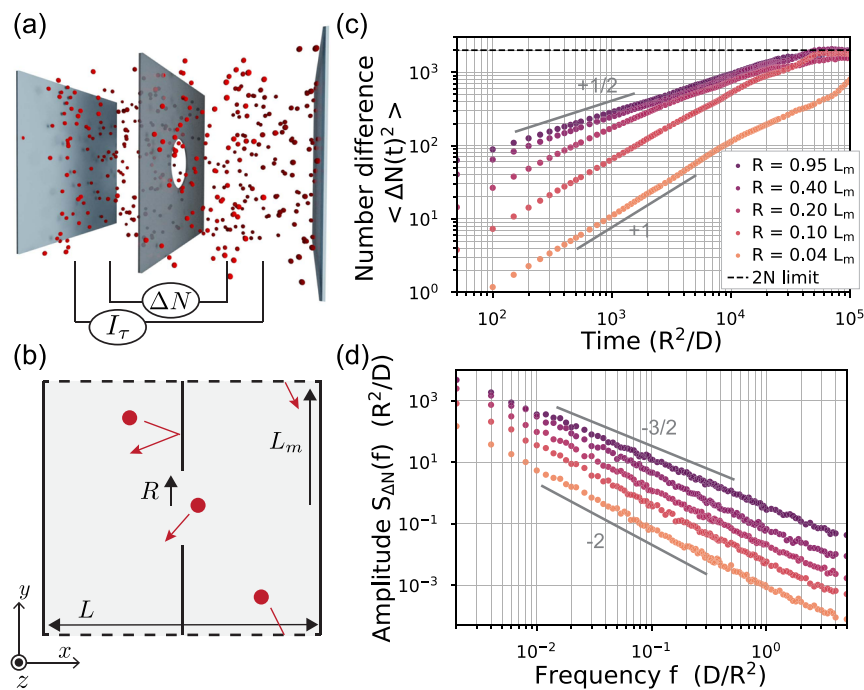


FIG. 1. Fractional noise in a simple nanoporous system: (a) Brownian dynamics of non-interacting particles (red spheres). Particles cross the wall through a circular pore of radius R . (b) Corresponding schematic with simulation parameters and details. Dashed (respectively, full) lines denote periodic (respectively, reflecting) boundaries. (c) Mean square concentration difference $\langle \Delta N^2(t) \rangle$ with time for different values of the pore size. (d) Corresponding frequency spectrum—shared legend with (c). Data points correspond to $N = 1000$ Brownian walkers simulated in a box of size $L = 500 R$. Values of L_m with respect to R are indicated in the labels. The total simulation time is $1.5 \times 10^6 R^2/D$ with a time step of $\Delta t = 0.05 R^2/D$.

conditions, a membrane with multiple nearby pores). When $R \ll L_m$, this corresponds to a small pore (or a membrane with isolated pores).

The finite extent of the reservoirs is modeled by a reflection boundary condition at $x = \pm L/2$ parallel to the membrane. Our simulation setting therefore allows us to probe the effect of pore size and reservoir size on translocation processes. Unlike other studies introducing effective boundary conditions to model the effect of reservoirs,^{33,41} here, we directly probe the effect of the *presence* of reservoirs on the system by fully accounting for them. Note that in the following, the most striking effects will arise from the presence of reservoirs, in that they allow for exchanges of particles between pore and reservoir regions, and not as much from their finite extent.

The N particles are modeled as Brownian walkers. The displacement of each walker during a time Δt is given by

$$\Delta \mathbf{X}_k = \sqrt{2D\Delta t} \mathbf{W}_k, \quad (1)$$

where \mathbf{W}_k are Gaussian random variables with mean $\langle \mathbf{W}_k \rangle = 0$ and variance $\langle W_k^i W_l^j \rangle = \delta_{ij} \delta_{kl}$ and $\langle \cdot \rangle$ are averages over realizations of the noise. Here, $\mathbf{X}_k = (x_k, y_k, z_k)$ is the position of a walker, where k is the running index over time, such that time is $t = k\Delta t$.

We introduce $\Delta N(t) = N_R(t) - N_L(t)$ as the difference between the number of particles to the right of the membrane (particles for which $x_k > 0$) vs particles to the left ($x_k < 0$). We are interested in the statistics of this random variable ΔN , notably because it represents the concentration difference between both sides and, thus, is linearly related to the osmotic pressure (at small concentration differences).³⁸

C. Summary

This paper is organized as follows.

In Sec. II, we explain in detail the emergence of fractional noise [$\langle \Delta N^2(t) \rangle \sim \sqrt{t}$] in the simple setting of a fully open membrane [corresponding to the large pore regimes, $R \sim L_m$, purple in Figs. 1(c) and 1(d)]. This setup is equivalent to studying Brownian walkers on a line. We rationalize fluctuations, correlation functions, and spectrum properties of both the number particle difference and current observables. The most important finding here is that fractional noise emerges spontaneously when studying *random particles crossing from one region to another*—here, from the left to the right. As a consequence, we expect fractional noise to be universal and emerge

in many different settings, which we investigate in the Secs. III and IV.

In Sec. III, we investigate how these results are maintained when the particles can only cross through narrow pores. We also introduce the mapping of the 3D geometry to a 1D problem. This allows us to fully rationalize the different behaviors obtained in Figs. 1(c) and 1(d). The key takeaway here is that different behaviors are obtained not only with the pore size but also, especially, in time. In general, in contrast with large pores, small pores $R \ll L_m$ exhibit diffusive noise over longer time scales. Yet, within specific time windows, *fractional noise may also be observed across all pore sizes*.

In Sec. IV, we investigate how fractional noise impacts long channels. Importantly, when the pore is long, it is possible to track the number of particles within the pore, akin to the number of charge carriers responsible for ionic conductance in ionic systems. We focus mainly on the noise properties of this number in this section. Because of its intrinsic nature, fractional noise is also observed in the number of particles within the pore. Interestingly, the noise spectrum of the number of particles within the pore exhibits not only power laws expected for fractional noise but also an additional $1/f^{1/2}$ power law scaling over a range of smaller frequencies.

In all sections, we discuss the results with the aim of optimizing the signal-to-noise ratio.

II. ORIGIN OF FRACTIONAL NOISE

A. Limit case of a wide pore: Walkers on a line

To understand the emergence of fractional noise in nanopores, we focus first on a limit case. Figure 1(c) shows that fluctuations in the number difference grow as $\langle \Delta N^2(t) \rangle \sim t^{1/2}$ predominantly for wide pores $R \sim L_m$. In this limit ($R \sim L_m$), we can consider as a first approximation that there is no physical membrane. Solute particles are diffusing, and we consider their probability of crossing the now “imaginary” wall at $x = 0$. Everything now happens as if the particles were walking on a line—see Fig. 2(a).

B. Number difference

In average, $\langle \Delta N(t) \rangle = 0$. To further quantify the fluctuations of $\Delta N(t)$, we, therefore, turn to its correlation function $\langle \Delta N(t) \Delta N(0) \rangle$. ΔN can be conveniently written as $\Delta N(t + \Delta t) = \Delta N(t) + 2I_{\Delta t}(t)\Delta t$, where $I_{\Delta t}(t)$ corresponds to the *net* current of

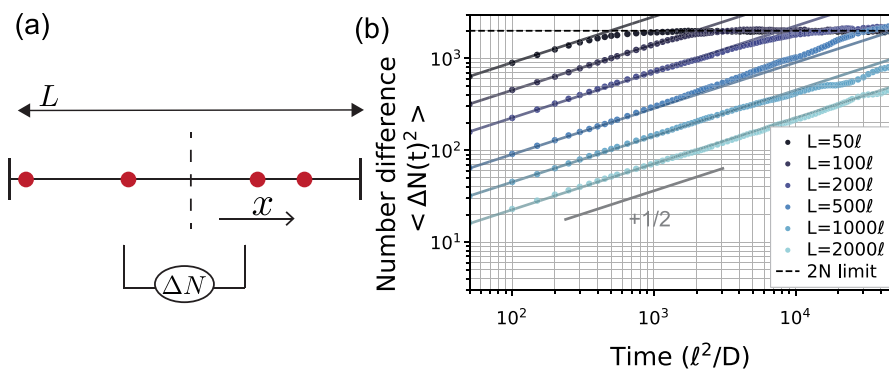


FIG. 2. Fractional noise for the concentration difference on a line. (a) Illustration of random walkers on a line. Red particles can cross the imaginary boundary at the center. (b) Mean square concentration difference $\langle \Delta N^2(t) \rangle$ with time for different values of box size L . Dots correspond to BD simulations and full lines to Eq. (9). Here, $N = 1000$ particles were simulated and ℓ is an arbitrary unit length. The total simulation time was $1.5 \times 10^6 \ell^2/D$ with a time step $\Delta t = 0.05 \ell^2/D$.

(uncharged) particles crossing the boundary $x = 0$ between t and $t + \Delta t$. A particle that started in $x < 0$ (respectively, $x > 0$) at time t and finds itself in $x > 0$ (respectively, $x < 0$) at time $t + \Delta t$ will contribute $+1/\Delta t$ (respectively, $-1/\Delta t$) to the current. Note that the definition of such a current does not pose any mathematical pathology. Although a Brownian walker does cross a boundary infinitely many times during Δt , here, $I_{\Delta t}(t)$ is finite since it counts whether the walker effectively crossed (for example, a particle crossing three times back and forth will contribute $+1 - 1 + 1 = 1$ time to the current).

Summing up over time, we obtain $\Delta N(t) = \Delta N(0) + 2 \sum_{k=0 \dots k} I_{\Delta t}(k \Delta t) \Delta t \rightarrow \Delta N(0) + 2 \int_0^t I(t_1) dt_1$ in the limit of small time steps. We can therefore write the correlation function for ΔN as

$$C(t, t') = \langle (\Delta N(t) - \Delta N(0))(\Delta N(t') - \Delta N(0)) \rangle = 4 \left\langle \int_0^t I(t_1) dt_1 \int_0^{t'} I(t_2) dt_2 \right\rangle. \quad (2)$$

We will write $\langle \Delta N^2(t) \rangle = \langle (\Delta N(t) - \Delta N(0))^2 \rangle$ in the following to lighten notations.

C. Statistics of the number difference

To determine the statistics of $\Delta N(t)$, it is therefore sufficient to find the statistics of $I(t)$. In the following, we will use a number of standard results for diffusing tracers in one dimension (for detailed proofs of these results, see Chaps. 2 and 3 of Ref. 42). We compute statistics by splitting the calculation into two parts:

1. Jumps on a common interval

We are first interested in the correlation function at equal times,

$$C_{\text{common}}(t) = 4 \left\langle \int_0^t I(t_1) dt_1 \int_0^t I(t_2) dt_2 \right\rangle. \quad (3)$$

As particles are uncorrelated, we can focus on a single particle.

We first derive the probability for the current to be $+1/\Delta t$ during Δt , meaning that the particle crossed from left to right. At any time t , the particle is evenly distributed between the left and right sides with a distribution $\rho_0(x) = 1/L$, where L is the domain size. In the following, we will assume $t \ll L^2/D$ to neglect boundary effects due to the finite extent of reservoirs. The full derivation accounting for these effects is reported in Appendix B and shows no difference at these timescales.

The probability that a step has size Δx during Δt is

$$p(s = \Delta x) = \frac{1}{\sqrt{4\pi D \Delta t}} e^{-\frac{\Delta x^2}{4D \Delta t}}, \quad (4)$$

and therefore, the probability that the particle made a step greater than Δx is

$$p(s \geq \Delta x) = \int_{\Delta x}^{\infty} p(s = s') ds' = \frac{1}{2} \left(1 - \operatorname{erf} \left(\frac{\Delta x}{\sqrt{4D \Delta t}} \right) \right), \quad (5)$$

where here the upper integration bound is not L but $+\infty$ as we neglect the finite extent of reservoirs. The probability that the current is $+1$ is equal to the probability that a particle came from the left and made it to the right,

$$p(I_{\Delta t} = +1/\Delta t) = \int_{-\infty}^0 \rho_0(x) p(s \geq -x) dx = \frac{1}{L} \sqrt{\frac{D \Delta t}{\pi}}. \quad (6)$$

Since the probability to observe current in one direction or the other is the same, we have $p(I_{\Delta t} = -1/\Delta t) = p(I_{\Delta t} = +1/\Delta t)$. In average, the current vanishes naturally, $\langle I(t) \rangle = 0$.

If now we consider a longer time interval t , the derivation does not change, and we can simply replace $\Delta t \rightarrow t$. The probability that the current integrated over time t is $+1$ is thus

$$p \left(\int_0^t I(t_1) dt_1 = +1 \right) = \frac{1}{L} \sqrt{\frac{Dt}{\pi}}, \quad (7)$$

and similarly for the reverse current. The equal time correlation for one particle therefore amounts to

$$\left\langle \int_0^t I(t_1) dt_1 \int_0^t I(t_2) dt_2 \right\rangle = (-1)^2 p \left(\int_0^t I(t_1) dt_1 = -1 \right) + (1)^2 p \left(\int_0^t I(t_1) dt_1 = +1 \right). \quad (8)$$

Using Eqs. (3) and (7) and multiplying by the number of (independent) particles, we find that

$$\langle \Delta N(t)^2 \rangle = C_{\text{common}}(t) = 8 \frac{N}{L} \sqrt{\frac{Dt}{\pi}} \sqrt{t}. \quad (9)$$

As expected, concentration fluctuations scale as $\langle \Delta N(t)^2 \rangle / N^2 \sim 1/N$. In small sized systems such as cells or nanofiltration devices, we therefore expect these fluctuations to be significant. The growth law [Eq. (9)] agrees perfectly with Brownian dynamics (BD) simulations, for very different numerical parameters—see Fig. 2(b) and Appendix A for simulation details. Interestingly, Eq. (9) shows that concentration fluctuations have large deviations with time. These deviations are eventually bounded by the system size—we turn to this limit next.

Limit value of fluctuations. At long enough times, the fluctuations are bounded. Indeed, at long times, we can write $N_L = n$ and $N_R = N - n$, where n is a binomial random variable. A total of N particles are placed on either side of the membrane with equal probability $p = 1/2$. n has a mean value $\langle n \rangle = pN = N/2$ and variance $\langle (n - \langle n \rangle)^2 \rangle = Np(1 - p) = N/4$. Thus, we can calculate

$$\langle \Delta N^2 \rangle = 2 \langle (N_R - N_L)^2 \rangle = 2 \langle (N - 2n)^2 \rangle = 2N. \quad (10)$$

The limit law [Eq. (10)] is consistently seen in our simulations—see Fig. 2(b).

The time t_{late} to reach saturation is set by equating Eqs. (9) and (10) such that $t_{\text{late}} = \frac{\pi L^2}{16 D}$. Naturally, this time corresponds to the typical time $\frac{L^2}{D}$ to diffuse to the boundaries of the domain. In experimental systems, the size of the reservoirs is typically $L = 1$ cm and $D \sim 2 \times 10^{-9}$ m²/s, yielding $t_{\text{late}} \sim 1$ h. Such square root noise dependence is therefore accessible to experimental systems.

2. Jumps on consecutive intervals

We are now interested in jumps on consecutive intervals of the correlation function, as

$$C_{\text{consecutive}}(t_1, t_2) = \left\langle \int_0^{t_1} I(t) dt \int_{t_1}^{t_1+t_2} I(t') dt' \right\rangle, \quad (11)$$

where the first interval is of length t_1 and the second interval is of length t_2 . For simplicity, we will write in this section $I^{(i)}$, the current on the i th interval. We focus as mentioned before on one particle. As we have shown in the previous paragraph, the probability that the integrated current is +1 during a length t_1 is $p(I^{(1)} = +1) = \sqrt{D t_1 / \pi}$. After that first jump, the particle is distributed as

$$\rho_1(x) = \frac{1}{2L} \sqrt{\frac{\pi}{D t_1}} \left(1 - \operatorname{erf} \left(\frac{x}{\sqrt{4D t_1}} \right) \right), \quad (12)$$

such that the probability that the particle crosses again (in the reverse direction) during the second time lapse t_2 is

$$\begin{aligned} p(I^{(2)} = -1 | I^{(1)} = +1) &= \int_0^\infty \rho_1(x) p(s \leq -x, t_2) dx \\ &= \frac{1}{2L} \left(1 + \sqrt{\frac{t_2}{t_1}} - \sqrt{1 - \frac{t_2}{t_1}} \right). \end{aligned} \quad (13)$$

The current correlations can be expressed in terms of the jump probabilities as

$$\begin{aligned} \langle I^{(2)} I^{(1)} \rangle &= -p(I^{(1)} = +1) p(I^{(2)} = -1 | I^{(1)} = +1) \\ &\quad - p(I^{(1)} = -1) p(I^{(2)} = +1 | I^{(1)} = -1), \end{aligned} \quad (14)$$

and coming back to N particles, we find that

$$C_{\text{consecutive}}(t_1, t_2) = -4 \frac{N}{L} \sqrt{\frac{D}{\pi}} (\sqrt{t_1} + \sqrt{t_2} - \sqrt{t_1 + t_2}). \quad (15)$$

Statistics of ΔN . Assembling the different jumps, we have $C(t, t') = C_{\text{common}}(t) + C_{\text{consecutive}}(t, t' - t)$, writing without loss of generality $t' > t$. We obtain

$$\langle \Delta N(t) \Delta N(t') \rangle = 4 \frac{N}{L} \sqrt{\frac{D}{\pi}} (\sqrt{t} + \sqrt{t'} - \sqrt{t' - t}). \quad (16)$$

Equation (16) is exactly the expectation value of a fractional Brownian walk⁴³ with Hurst index $H = 1/4$. This allows us to conclude that ΔN is a fractional Brownian walk with “diffusion coefficient” $\mathcal{D} = 4 \frac{N}{L} \sqrt{\frac{D}{\pi}}$. Notably, the emergence of such fractional noise is totally intrinsic and relies on no specific assumptions for the system. As such, it could serve as a remarkable textbook example for fractional or subdiffusive noise.

Note that Eq. (16) can be inferred in many different ways.^{39,40} The proof presented here—in contrast with other more formal proofs—sheds light on the *physical mechanisms* that result in such peculiar statistics, *namely, particles crossing forward and in a limited amount of time turning around and crossing back*. This is also at the basis of the current statistics, which we study in Sec. II D.

D. Current of (uncharged) particles

As most experimental apparatus are sensitive not to an instantaneous current but to a current integrated over a short time interval, say, τ , we define the experimentally relevant current (of uncharged particles) as

$$I_\tau(t) = \int_t^{t+\tau} I(t_1) dt_1. \quad (17)$$

Typically, $\tau^{-1} \sim 100$ kHz. In our non-dimensional time scales, with a typical length scale for nanopores $\ell \sim 10$ nm and $D = 10^{-9}$ m²/s, we have $\tau \sim 100 \frac{\ell^2}{D}$.

We now seek the correlations of $I_\tau(t)$. When $t \leq \tau$, we can split the correlation function calculation as

$$\begin{aligned} \langle I_\tau(t) I_\tau(0) \rangle &= \frac{1}{\tau^2} \left(\left\langle \int_t^\tau I(t_1) dt_1 \int_t^\tau I(t_2) dt_2 \right\rangle \right. \\ &\quad + \left\langle \int_t^\tau I(t_1) dt_1 \int_0^t I(t_2) dt_2 \right\rangle \\ &\quad \left. + \left\langle \int_\tau^{t+\tau} I(t_1) dt_1 \int_0^\tau I(t_2) dt_2 \right\rangle \right), \end{aligned} \quad (18)$$

such that we can use previous results on correlation functions on common and consecutive intervals. When $t > \tau$, another splitting may be done leading to a similar result such that the correlation is simply (for any time t)

$$\langle I_\tau(t) I_\tau(0) \rangle = \frac{N}{L \tau^2} \sqrt{\frac{D}{\pi}} (\sqrt{|t - \tau|} + \sqrt{t + \tau} - 2\sqrt{t}). \quad (19)$$

Equation (19) corresponds to a result derived in Ref. 44, for the velocity autocorrelation function of a fractional Brownian walker—up to subtleties associated with the different systems. Here, current $I(t)$ plays the role of the velocity since it is the derivative of the number difference $\frac{d\Delta N(t)}{dt} = 2I(t)$. Equation (19) agrees perfectly with BD simulations—see Fig. 3(a). Notably, it features a *negatively correlated* peak. This peak corresponds to particles that cross, turn around, and cross back again. The maximum value of the negative peak is achieved in $t = \tau$ and is of significant magnitude since $\frac{\langle I_\tau(t) I_\tau(0) \rangle}{\langle I_\tau(0)^2 \rangle} \simeq -0.3$ regardless of the system specifics.

We now turn to exploring the typical signature of the noise in the current spectrum.

E. Spectrum of fluctuations

We define the spectrum of a random variable X as

$$S_X(f) = \lim_{T \rightarrow \infty} \left\langle \frac{1}{T} \left| \int_0^T e^{i2\pi f t} X(t) dt \right|^2 \right\rangle. \quad (20)$$

Our simulations are long enough that we need not account for finite acquisition time effects.⁴⁵

1. Number difference spectrum

As the number difference ΔN may drive currents in more complex systems (e.g., osmotic currents), we investigate its spectrum. From Eq. (16), we obtain⁴⁵

$$S_{\Delta N}^{(\text{line})}(f) = \frac{2 N \sqrt{2D}}{L} \frac{1}{(2\pi)^{3/2}} \frac{1}{f^{3/2}}. \quad (21)$$

The spectrum of the noise, therefore, has a low frequency decay as $1/f^{3/2}$ —consistently seen in simulations; see Fig. 3(b) (blue curves).

2. Spectrum of particle current

The spectrum of the particle current is easily calculated from Eq. (19) as

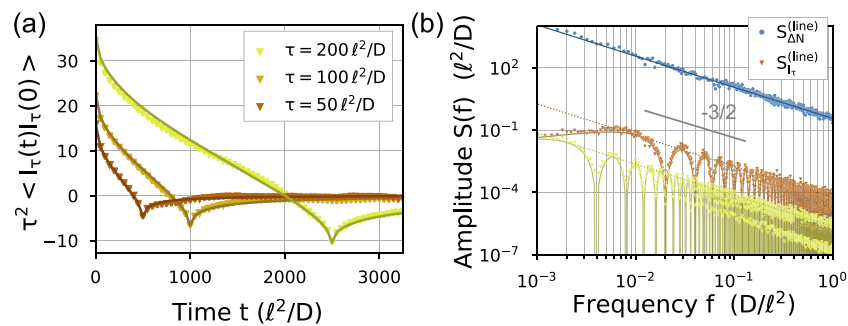


FIG. 3. Current fluctuations (of uncharged particles) on a line. (a) Autocorrelation function of the current from BD simulations on a line (dots, multiplied by the integration time τ^2 for more clarity on a single plot). The full lines correspond to Eq. (19). (b) Spectrum of fluctuations for the number difference ΔN and two of the current traces I_r shown in (a). The full blue line corresponds to Eq. (21), and the full maroon and green lines correspond to Eq. (22) [the dashed lines correspond to Eq. (22), taking the sinusoidal multiplicative factor $\sin^2(2\pi f\tau) \equiv 1$ to show the power law decay]. Numerical parameters correspond to that of Fig. 2.

$$S_{I_{\text{tau}}}^{(\text{line})}(f) = \frac{N}{L\tau^2} \sqrt{\frac{D}{\pi}} \frac{\sin^2(2\pi f\tau)}{(2\pi)^{3/2}} \frac{1}{f^{3/2}}. \quad (22)$$

We again find a low frequency decay as $1/f^{3/2}$, also seen in simulations; see Fig. 3(b).

Statistics of particles on a single line decisively point to a low frequency noise scaling as $1/f^{3/2}$. This noise simply originates from particles crossing from one region to another. In nanoporous systems, particles continuously cross from the reservoir to the pore area and back. We therefore expect such *intrinsic* fractional noise to leave traces. Nanoporous systems are yet more complex than the simple line problem. In Secs. II and IV, we investigate how these results hold or change in more realistic geometries.

III. FRACTIONAL NOISE IN NARROW PORES

When the pore mouth is extremely small, a regime different from fractional noise is expected. In fact, we expect the *return probability* of crossing particles to vanish as the opening is so narrow that particles cannot find it again in finite time. Simulations show

that $\langle \Delta N^2(t) \rangle \sim t^{0.5-1}$. However, there is no systematic way of understanding the fluctuations of ΔN for narrow pores. This is the purpose of Sec. III A.

A. Mapping to a simpler problem

We focus on the case of short pores—as depicted in Fig. 1. Seeking solutions as in Sec. II of the full problem is tedious and greatly dependent on the specific geometry of the pore. Instead, we map the open pore problem to a simpler model that features similar equilibrium characteristics—see Fig. 4(a).

In this setup—termed, henceforth, the *rates model*—a particle performs a random walk freely on a *passing* line [corresponding to the open pore cylinder—see shaded green in Fig. 4(a)]. The particle can transition with rate q_{off} to a *blocked* line with a reflecting wall in the center (corresponding to the membrane wall). The particle transitions back to the open line with rate q_{on} . The rates have to obey detailed balance

$$q_{\text{on}} \mathcal{A}_{\text{closed}} = q_{\text{off}} \mathcal{A}_{\text{open}}, \quad (23)$$

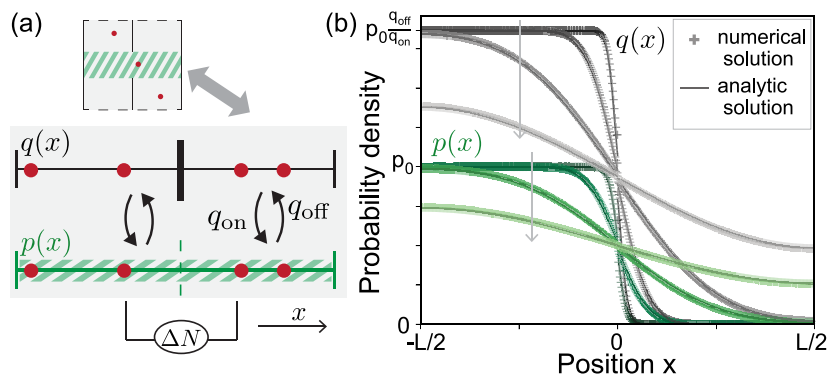


FIG. 4. Mapping of a 3D problem to the—easy to solve—rates model. (a) Sketch of the model: walkers (red) perform a Brownian walk on two adjacent lines. On the black line, walkers cannot cross at the center. Walkers can swap lines with rates q_{on} and q_{off} . (b) Probability density for the particles on the crossing line [$p(x)$] and on the blocked line [$q(x)$] starting on the left. Finite difference numerical solutions (dots, see Appendix A) and analytic solutions of Eq. (25) are presented. Arrows indicate the direction of time, and profiles are represented, respectively, at $t = 50, 500, 5000, 25000 R^2/D$. Here, $2R = 3L_m$ such that $q_{\text{off}} \approx 1.86q_{\text{on}}$.

where \mathcal{A}_i are the areas corresponding to the closed or open parts of the membrane. In the case of the circular pore of radius R on a membrane square of size $2L_m \times 2L_m$, we get

$$\frac{q_{\text{on}}}{q_{\text{off}}} = \frac{\mathcal{A}_{\text{open}}}{\mathcal{A}_{\text{closed}}} = \frac{\pi R^2}{4L_m^2 - \pi R^2}. \quad (24)$$

Let $p(x, t)$ and $q(x, t)$ be the probability that a particle is in the passing or blocked state at position x and time t , respectively. They obey the coupled set of equations

$$\begin{cases} \partial_t p = -q_{\text{off}} p + q_{\text{on}} q + D \partial_{xx} p, \\ \partial_t q = +q_{\text{off}} p - q_{\text{on}} q + D \partial_{xx} q \end{cases} \quad (25)$$

with reflection boundary conditions on all walls $\partial_x q|_{x=0^\pm} = 0$, $\partial_x p|_{x=\pm L/2} = \partial_x q|_{x=\pm L/2} = 0$. q (but not p) is discontinuous in $x = 0$. To infer the probability that, for example, the particle made it to the right starting from the left during time t , we can choose initial conditions where the particle is distributed uniformly and in an equilibrium way on the left. This amounts to $p(x, t = 0) = p_0 \Theta(x < 0)$ and $q(x, t = 0) = q_{\text{off}}/q_{\text{on}} p(x, t = 0)$, where $p_0 = \pi R^2/4L_m^2 L$ and Θ is the Heaviside function. The probability that the particle made it to the other side at time t is then

$$p\left(\int_0^t I(t_1) dt_1 = +1\right) = \int_0^{L/2} [p(x, t) + q(x, t)] dx. \quad (26)$$

Finally, we obtain the statistics of ΔN as

$$\langle \Delta N^2(t) \rangle = 2 \times 2^2 \times N \times p\left(\int_0^t I(t_1) dt_1 = +1\right). \quad (27)$$

Framed as such, the *rates model* has the same equilibrium characteristics as the 3D pore. We therefore expect to recover similar noise features and to be able to explain their dependencies. Eventually, we will show that the rates model reproduces exactly the results of 3D Brownian dynamics (BD) simulations.

B. Solving the rates model

Analytic solutions to the rates model defined by Eq. (25) can be found in Laplace space. The method and results are reported in [Appendix B](#). Analytic solutions are in perfect agreement with numerical finite difference solutions of the partial differential equations—see [Fig. 4\(b\)](#). We find that

$$\mathcal{L}[\langle \Delta N^2 \rangle](s) = \frac{4N}{L} \frac{q_{\text{on}}}{q_{\text{off}} + q_{\text{on}}} \frac{\sqrt{D}}{s^{3/2}} \frac{1 + \frac{q_{\text{on}}}{q_{\text{off}}}}{\sqrt{\frac{s}{s+q_{\text{on}}+q_{\text{off}}} + \frac{q_{\text{on}}}{q_{\text{off}}}}}, \quad (28)$$

where \mathcal{L} is the Laplace transform, s is the Laplace frequency, $q = \sqrt{s/D}$, and $\tilde{q} = \sqrt{s/D + (q_{\text{on}} + q_{\text{off}})/D}$. Here, Eq. (28) is written at times $t \ll L^2/D$, corresponding to a large box L . Equation (28) does not have an analytic form in real time (to the best of our knowledge). However, we may infer limiting behaviors in real time for a few relevant cases.

C. Narrow pore regime ($R \ll L_m$)

When $q_{\text{off}} \gg q_{\text{on}}$ (for the narrow pore $R \ll L_m$), we obtain an analytic expression in real time as

$$\langle \Delta N^2(t) \rangle = \frac{4N}{L} \frac{\pi R^2}{4L_m^2} \left[\sqrt{\frac{Dt}{\pi}} e^{-(q_{\text{on}} + q_{\text{off}})t} + \frac{\sqrt{D}\left(\frac{1}{2} + (q_{\text{on}} + q_{\text{off}})t\right)}{\sqrt{q_{\text{on}} + q_{\text{off}}}} \text{erf}\left(\sqrt{(q_{\text{on}} + q_{\text{off}})t}\right) \right]. \quad (29)$$

1. Early times, $t \ll t_{\text{early}} = (q_{\text{off}} + q_{\text{on}})^{-1}$

At very short times $t \ll t_{\text{early}} = (q_{\text{off}} + q_{\text{on}})^{-1} \sim R^2/D$, we find (using the circular pore expressions for q_{on} and q_{off}) that

$$\langle \Delta N^2(t) \rangle_{t \ll t_{\text{early}}} = \frac{8N}{L} \frac{\pi R^2}{4L_m^2} \sqrt{\frac{Dt}{\pi}}. \quad (30)$$

The fluctuations here are exactly that of a walk on a line corrected by a “geometric” prefactor $\frac{\mathcal{A}_{\text{open}}}{\mathcal{A}_{\text{closed}}} = \frac{\pi R^2}{4L_m^2}$ accounting for the open area of the membrane. In fact, at early times, the particles that participate to the fluctuations are only those that are found very close to the pore—see the blue region in [Fig. 5\(a\)](#). They thus behave exactly as if they were “seeing” no membrane wall—yet. This fractional behavior is seen systematically at early times for all pore sizes—see [Fig. 5\(b\)](#).

2. Intermediate times, $t_{\text{early}} \ll t \ll t_{\text{int}}$

At intermediate times, namely, when exchanges are now possible between domains in front of the pore and facing the wall $t_{\text{early}} \ll t \ll t_{\text{int}}$ (the limit t_{int} will be defined in the following paragraph), we find a diffusive regime

$$\langle \Delta N^2(t) \rangle_{t_{\text{early}} \ll t \ll t_{\text{int}}} = \frac{4N}{L} \frac{\pi R^2}{4L_m^2} \sqrt{D q_{\text{off}}} t. \quad (31)$$

Here, particle translocation events are dominated by exchanges between the pore region and the rest of the reservoirs—see purple in [Fig. 5](#). Equation (31) can be further interpreted as an actual random walk. When the opening of the pore is quite small, during the characteristic time $\tau_{\text{off}} = 1/q_{\text{off}}$, a small quantity of particles may transition from one side to the other with probability $\delta p = \frac{N}{2} \frac{\delta \mathcal{V}}{\mathcal{V}}$, where $\mathcal{V} = 4L_m^2 L$ is the total volume and $\delta \mathcal{V}$ is a small volume in front of the pore mouth. This volume writes naturally $\delta \mathcal{V} = \pi R^2 \ell_{\text{off}}$, where $\ell_{\text{off}} = \sqrt{D/q_{\text{off}}}$ is a relevant length scale inside the reservoirs. Particles further than ℓ_{off} from the pore mouth will in average not make it through the pore. If that small quantity of particles shifts right, then $\Delta N = +2$ with probability δp and -2 with same probability. The steps in ΔN are uncorrelated; after time τ_{off} , particles in front of the pore have been remixed within the reservoirs and replaced by others. Therefore, ΔN is a Brownian walk with time steps τ_{off} and step sizes of ± 2 with probability δp . We find that

$$\langle \Delta N^2(t) \rangle = 2^2 \times 2\delta p \times \frac{t}{\tau_{\text{off}}}, \quad (32)$$

and gathering all quantities, we recover Eq. (31). Such diffusive behavior is also seen systematically at intermediate times for nearly all pore sizes—see [Fig. 5\(b\)](#).

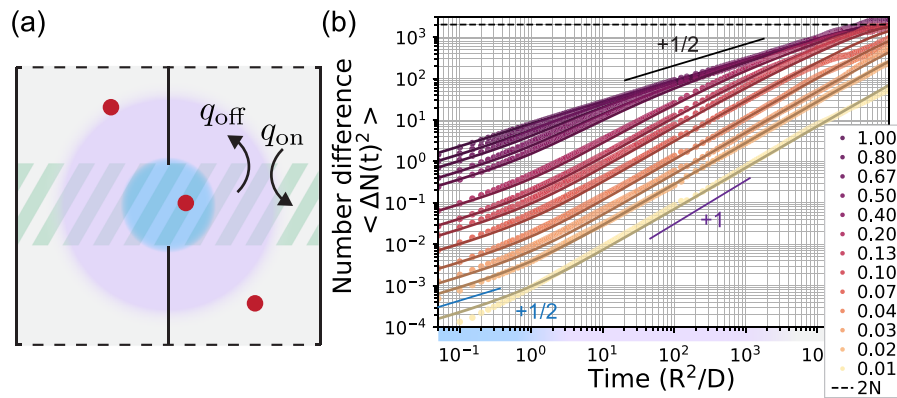


FIG. 5. Mechanism for particle fluctuations across a 3D nanopore. (a) Sketch of the different fluctuation regimes for a small pore: the early regime in blue corresponds to particles located close to the pore mouth, the intermediate regime in purple corresponds to exchanges between the open pore region (dashed green) and the rest of the reservoir, and the later regime in gray corresponds to a well-mixed situation. (b) Number difference fluctuations with time for several values of R/L_m as indicated with the various colors. Dots correspond to data from BD, and lines correspond to the analytic solution of Eq. (25). Matching at very early times and very narrow pores is not perfect due to a lack of significant statistics when only a few particles translocate. The regimes are identified with the same color scheme as in (a). Simulation parameters correspond to Fig. 1.

3. Later times, $t \gg t_{int}$

At later times, starting from Eq. (28) we find, in general, (regardless of the pore size) $\mathcal{L}[\langle \Delta N^2 \rangle](s) \underset{s \rightarrow 0}{=} \frac{4N}{L} \frac{\sqrt{D}}{s^{3/2}}$, yielding

$$\langle \Delta N^2(t) \rangle_{t \gg t_{int}} = \frac{8N}{L} \sqrt{\frac{Dt}{\pi}}. \quad (33)$$

At later times, whatever the size of the pore, we recover the bare fractional noise. This later regime corresponds to a phase where the reservoir is now sufficiently well mixed that it does not “matter” anymore whether particles are in front of the open pore or not. This later regime may be observed only from times $t \geq t_{int}$, where t_{int} corresponds to the cross-over between the intermediate diffusive [Eq. (31)] and late fractional noise [Eq. (33)]. This leads to $t_{int} = \left(\frac{8L_m^2}{\pi^{3/2}R^2} \right)^2 \frac{1}{q_{off}}$. Note that it is only possible to observe this late time regime if $t_{int} \leq t_{late} \sim \frac{L^2}{D}$, the time when fluctuations reach the $2N$ limit. The later time regime is depicted in Fig. 5 in gray and is indeed reached for a number of pores.

4. Conclusion for narrow pores

The number difference ΔN in narrow pores therefore experiences four different phases:

- fractional noise (as \sqrt{t}) for $t \ll t_{early} \simeq \frac{R^2}{D}$,
- diffusive noise for $t_{early} \ll t \ll t_{int} \simeq \frac{L_m^4}{R^4} t_{early}$,
- fractional noise (as \sqrt{t}) for $t_{int} \ll t \ll t_{late} \simeq \frac{L^2}{D}$,
- saturation for $t \gg t_{late}$.

Note that here, the time to reach saturation of the fluctuations t_{late} depends, in general, on the pore size. For very small pore sizes, we can equate Eq. (31) with $2N$ to find that $t_{late} \sim \frac{L_m^2 L}{DR}$. As t_{late} scales inversely with the pore size, this increases the overall time scale over which such regimes may be observed experimentally.

D. Wide pore regime ($R \sim L_m$)

When $q_{off} \ll q_{on}$ (for wide pores $R \sim L_m$), $\mathcal{L}[\langle \Delta N^2 \rangle](s) = \frac{4N}{L} \frac{\sqrt{D}}{s^{3/2}}$ such that we obtain for all times in very broad pores

$$\langle \Delta N^2(t) \rangle = \frac{8N}{L} \sqrt{\frac{Dt}{\pi}}. \quad (34)$$

We recover naturally the result for Brownian walk on a line.

E. Agreement with the 3D pore problem

To check how the rates model reproduces BD simulations through a 3D pore, we overlap predictions from the analytic solution of the rates model and BD results—see Fig. 5. To complete the mapping, we need to specify the value of the rates q_{on} and q_{off} . The phenomenological choice

$$q_{off}^{-1} = \frac{\pi R^2}{4D} \text{ and } q_{on}^{-1} = \frac{4L_m^2 - \pi R^2}{4D}, \quad (35)$$

obeys detailed balance Eq. (24). Here, we chose the rates as $q = a^2/4D$. a^2 corresponds to the characteristic area associated with the rate as expressed in Eq. (24). The factor $1/4$ corresponds to $1/2d$, where $d = 2$ is the dimension of interest for diffusion parallel to the membrane plane. Such a phenomenological choice accurately reproduces BD simulations—see Fig. 5(a). The agreement is excellent over six orders of magnitude in time and for many pore parameters. Figure 5 highlights the different regimes (early fractional, intermediate diffusive, and later fractional). In particular, at later times, for a few intermediate pores ($R \sim 0.2\text{--}0.5L_m$), fractional noise is indeed observed again after a diffusive interval.

Importantly, the rates model is not specific to the circular geometry of the pore and would hold for other geometries such as squares (see Appendix C) or rectangular slits.

F. Noise spectrum in nanopores

1. Noise spectrum

Analysis of the different regimes in time of ΔN allows us to draw conclusions on the noise spectrum of ΔN or I_τ . Here, for simplicity, we focus on the noise spectrum properties of ΔN . Similarly, as for $S_{\Delta N}$, in the case of the single line, we can use the results of Ref. 44,

- at high frequencies (early times), we have

$$S_{\Delta N}(f) \underset{f \gg t_{\text{early}}^{-1}}{=} \frac{\pi R^2}{4L_m^2} \frac{2N\sqrt{2D}}{L(2\pi)^{3/2}} \frac{1}{f^{3/2}} = \frac{\pi R^2}{4L_m^2} S_{\Delta N}^{(\text{line})}(f), \quad (36)$$

- at intermediate frequencies,

$$S_{\Delta N}(f) \underset{t_{\text{early}}^{-1} \gg f \gg t_{\text{int}}^{-1}}{=} \frac{\pi R^2}{4L_m^2} \frac{8N}{L} \frac{\sqrt{Dq_{\text{off}}}}{(2\pi)^2} \frac{1}{f^2}, \quad (37)$$

- at low frequencies (at late times or if the pore size/pore density is large enough),

$$S_{\Delta N}(f) \underset{f \ll t_{\text{int}}^{-1}}{=} \frac{2N\sqrt{2D}}{L(2\pi)^{3/2}} \frac{1}{f^{3/2}} = S_{\Delta N}^{(\text{line})}(f). \quad (38)$$

The regimes decaying as $1/f^\alpha$ with $\alpha = 3/2$ or 2 are consistently observed in Fig. 6 for the variety of pores investigated. The transitions from one regime to another are smooth. As a result, extracting the exponent α over a finite frequency range (Fig. 6, inset) can result in the observation of α values continuously ranging between 1.5 and 2.0. This hints that in experimental conditions, where acquisition times are finite, similar real valued exponents could be observed.

2. Optimizing signal-to-noise ratio in short pores

a. *Currents driven by an external field.* In most nanoporous systems, currents are driven by an external field, say, E . For example, ionic currents are driven by an electric field. Instead of deriving the full consequences of an applied field on the fluctuations, here, we

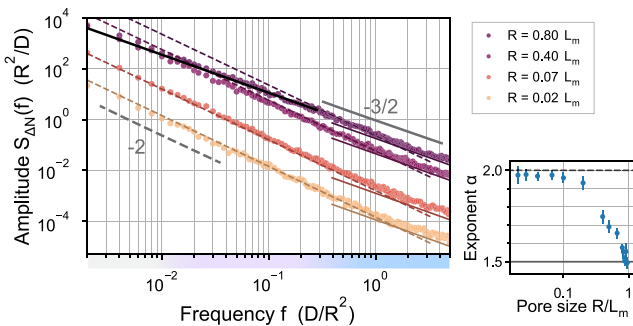


FIG. 6. Noise spectrum in narrow short pores. Noise spectrum amplitude of the number difference in units of time R^2/D for various pore sizes R . Dots correspond to BD data, and lines correspond to analytic results for the low frequencies [thick full black line, Eq. (36)], intermediate frequencies [dashed, color coded, Eq. (37)], and high frequencies [full, color coded, Eq. (38)]. The different regimes are highlighted with the same color code in the frequency spectrum, as in Fig. 5. (Inset) Least-squares fit to find the power law exponent α in $S_{\Delta N}(f) \sim 1/f^\alpha$ over the low frequency range ($f \leq 0.03D/R^2$). Simulation parameters correspond to that of Fig. 1.

make a simple reasoning to infer the expected signal-to-noise ratio in the linear response regime.

With an applied field, we expect to measure an average current of particles scaling as $\langle I_{\text{ext}} \rangle = \mathcal{G}E$, where E is the driving force and \mathcal{G} is the pore's conductance, taking into account the geometric parameters of the system. Typically,¹⁶ for electric fields, we expect $\mathcal{G} \sim R^2$. As a consequence, we obtain (within the linear response regime) that

$$\frac{\langle \delta I_{\text{ext}}^2 \rangle}{\langle I_{\text{ext}} \rangle^2} = \frac{\langle I_\tau^2 \rangle}{\mathcal{G}^2 E^2} \sim \begin{cases} \frac{1}{R^2} & \text{for } f \ll t_{\text{int}}^{-1} \\ \frac{1}{R^4} & \text{for } f \gg t_{\text{int}}^{-1} \end{cases}, \quad (39)$$

depending on the range of frequencies under scrutiny. Here, $\delta I_{\text{ext}} = I_{\text{ext}} - \langle I_{\text{ext}} \rangle$ corresponds to current fluctuations with respect to the mean, and we used the scaling laws in Eqs. (36)–(38). In this setting, we find that wide pores are required to maximize the signal-to-noise ratio.

b. *A note on osmotic currents.* Although it remains to be assessed in more advanced simulation frameworks (taking explicitly into account the solvent and its differential interaction with the membrane), we expect fluctuations of the number difference, corresponding to the concentration difference, to induce fluctuations in the osmotic pressure drop (at small concentration differences at least) and, therefore, in osmotic driven currents. We therefore make a short reasoning to infer the signal-to-noise ratio here. When a concentration difference, say, ΔN_0 is applied between the two pore sides, we expect a resulting osmotic current³⁸ in average as $\langle I_{\text{osm}} \rangle \propto \Delta N_0$. Osmotic current fluctuations therefore scale as

$$\frac{\langle \delta I_{\text{osm}}^2 \rangle}{\langle I_{\text{osm}} \rangle^2} = \frac{\langle \Delta N^2 \rangle}{\Delta N_0^2} \sim \begin{cases} \frac{R^2}{L_m^2} & \text{for } f \ll t_{\text{int}}^{-1} \\ 1 & \text{for } f \gg t_{\text{int}}^{-1} \end{cases}, \quad (40)$$

where we made use of the scaling laws in Eqs. (36)–(38). To maximize the signal-to-noise ratio, here, narrow pores, or pores in low density on the membrane, can be used.

Overall, in short pores, fractional noise remains predominant at high and low frequencies, while diffusive noise occurs at intermediate frequencies. This results in noise spectral densities scaling as $1/f^{3/2}$ and $1/f^2$. Optimizing the signal-to-noise ratio strongly depends on the type of current investigated. Beyond the short pore regime explored here, long pores (typically, at least as long as they are wide) are also common in biological and artificial nanoporous systems. The purpose of Sec. IV is to identify how fractional noise impacts these long channels.

IV. NANOCHANNELS, NUMBER OF “CHARGE CARRIERS,” AND EMERGENCE OF $1/f^{1/2}$ NOISE

We now investigate geometries where the pore has a finite length L_0 —see Fig. 7. We refer to these systems as *nanochannels* in contrast with *nanopores*, which are infinitely short. Importantly, here, we may define the number of (uncharged) particles within the pore N_c , akin to the “number of charge carriers”—in analogy with ionic solutions where electric conductance is directly related to the number of charge carriers.⁴⁶ We wish to understand what scalings we can expect in the noise, especially for the number of particles within the pore N_c .

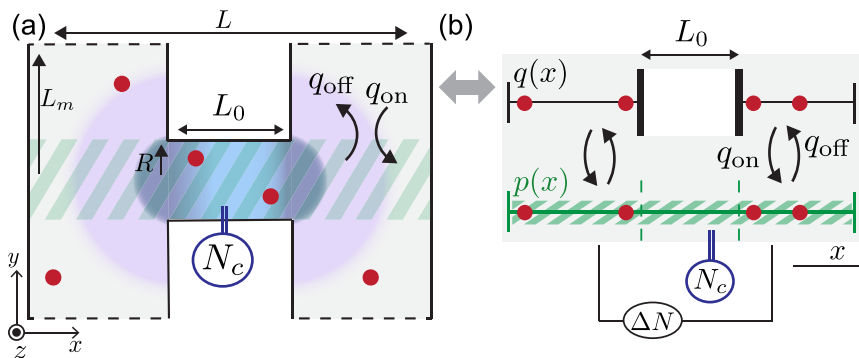


FIG. 7. 3D nanochannel noise regimes and mapping to a rates model. (a) 3D nanochannel geometry and different fluctuation regimes for a small pore: the initial regime (dark gray) corresponds to particles located close to the pore mouths, the early regime (lighter blue) corresponds to particles all along the channel and close to the pore mouths, the intermediate regime (purple) corresponds to exchanges between the open pore region (dashed green) and the rest of the reservoir, and the later regime in gray corresponds to a well-mixed situation. (b) Mapping of a 3D nanochannel to a rates model similar to that of Fig. 4.

A. Very long nanochannels

As a simplistic yet insightful introduction to nanochannels, we consider “channels” on a line—see Fig. 8(a), similar to the treatment of Sec. II. On this line, the channel is delimited by two imaginary boundaries in $x = \pm L_0/2$, where L_0 is the length of the channel. In BD simulations, we still use reflecting boundary conditions in $x = \pm L/2$ to mimic the effect of reservoirs. For simplicity, in analytic derivations, we assume $L_0 \ll L$ and we neglect the influence of boundaries.

1. Number difference

The relevant number difference corresponds now to the difference in particle number between the right and left sides $\Delta N = N(x > L_0/2) - N(x < -L_0/2)$. Similarly, as in Sec. II, this problem is amenable to analytic calculations. The fluctuations of ΔN are easily expressed in terms of the probability to make jumps from one area to another, with the added complexity that different jumps contribute differently to ΔN . Particles jumping from the left to the right (or inversely) will make a change $+2$ to ΔN (red arrow), while

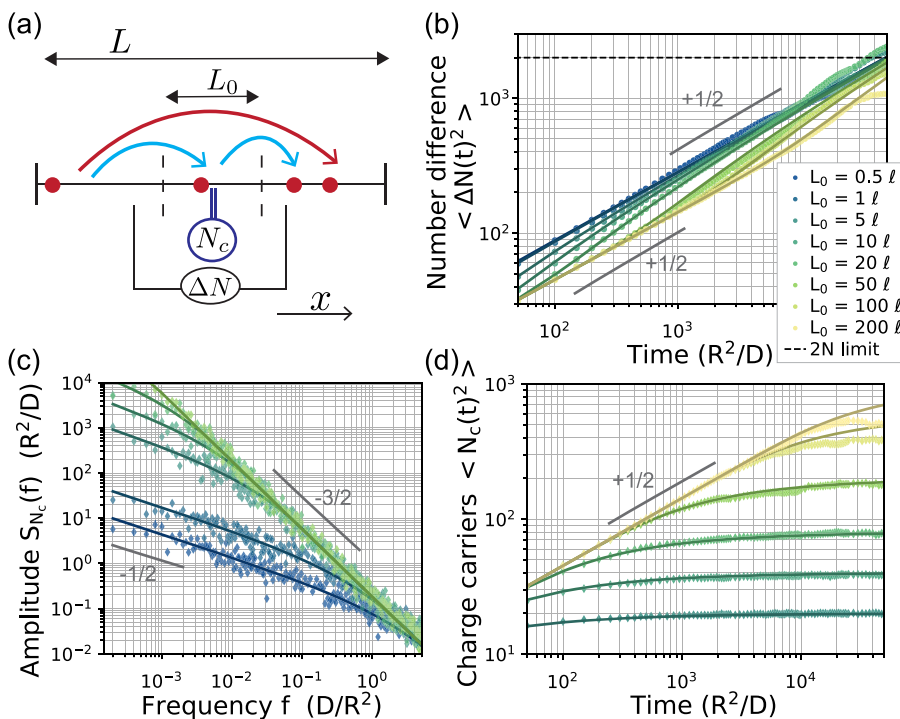


FIG. 8. Fractional noise in long channels. (a) Illustration of long channels, where we consider particle number difference ΔN between the left and right sides of imaginary boundaries in $x = \mp L_0/2$, respectively. We also consider the number of particles N_c inside the channel with $-L_0/2 < x < L_0/2$. Color arrows indicate all jumps to the right contributing to ΔN or to N_c . (b) Mean square number difference $\langle \Delta N^2(t) \rangle$, and (d) the number of particles within the pore $\langle N_c^2(t) \rangle$ with time for different values of the channel size L_0 . Dots are BD data, and lines correspond to Eq. (46) for (b) and Eq. (50) for (d). Slight mismatch at the largest times can be explained by limited data statistics. (c) Corresponding spectrum S_{N_c} for the number of particles within the channel. Lines correspond to Eq. (56). Legend for the size of the channel L_0 is shared between panels (b)–(d). Simulation parameters correspond to that of Fig. 2. $N = 1000$ particles were simulated, and ℓ is an arbitrary length unit. The total simulation time is $1.5 \times 10^6 \ell^2/D$ with a time step $\Delta t = 0.05 \ell^2/D$.

particles jumping in and out of the channel will only contribute +1 to ΔN (blue arrows)—see Fig. 8(a). As in Sec. II, to make analytic derivations simpler, we focus on times $t \ll L^2/D$ such that we can neglect the finite extent of reservoirs.

We focus on all the jumps toward the right. The probability distribution of the particle's position, provided that it started on the left ($x < -L_0/2$), is

$$p_L(x, t) = \frac{\rho_0}{2} \left[1 - \operatorname{erf} \left(\frac{x + L_0/2}{\sqrt{4Dt}} \right) \right], \quad (41)$$

where $\rho_0 = N/L$ is the concentration of particles. The probabilities to jump from the left (L) to the channel (C) or to the right (R) are

$$p_{L \rightarrow C}(t) = \int_{-\frac{L_0}{2}}^{\frac{L_0}{2}} p_L(x, t) dx, \quad p_{L \rightarrow R}(t) = \int_{\frac{L_0}{2}}^{+\infty} p_L(x, t) dx, \quad (42)$$

where here the upper integration bound is $+\infty$ not L as we may neglect the finite extent of reservoirs at short enough times.

If the particle started in the center, the probability distribution of its position is

$$p_C(x, t) = \frac{\rho_0}{2} \left[\operatorname{erf} \left(\frac{x + L_0/2}{\sqrt{4Dt}} \right) + \operatorname{erf} \left(\frac{L_0/2 - x}{\sqrt{4Dt}} \right) \right], \quad (43)$$

and the probability to jump from the center to the right is

$$p_{C \rightarrow R}(t) = \int_{\frac{L_0}{2}}^{+\infty} p_C(x, t) dx. \quad (44)$$

Finally, the fluctuations sum up to

$$\langle \Delta N^2(t) \rangle = 2(2^2 p_{L \rightarrow R}(t) + 1^2 p_{L \rightarrow C}(t) + 1^2 p_{C \rightarrow R}(t)), \quad (45)$$

where factor 2 in front of the whole expression originates from the fact that particles may jump with equal probability right or left. We stress again that we abbreviate here $\langle \Delta N^2(t) \rangle = \langle (\Delta N(t) - \Delta N(0))^2 \rangle$. Standard algebra yields

$$\langle \Delta N^2(t) \rangle = 2N_0 \left[\left(1 + e^{-\frac{L_0^2}{4Dt}} \right) \sqrt{\frac{4Dt}{\pi L_0^2}} - 1 + \operatorname{erf} \left(\frac{L_0}{\sqrt{4Dt}} \right) \right], \quad (46)$$

where $N_0 = \rho_0 L_0$. Equation (46) corresponds exactly with BD simulations (for $t \ll L^2/D$)—see Fig. 8(b). This problem may also be solved in Laplace space, with a similar framework as in Appendix B.

Interestingly, the fluctuations of ΔN feature two relevant limits. At early times, we find fractional noise

$$\langle \Delta N^2(t) \rangle \underset{t \ll L_0^2/D}{=} 4 \frac{N}{L} \sqrt{\frac{Dt}{\pi}}, \quad (47)$$

that is exactly 1/2 of that observed at longer times

$$\langle \Delta N^2(t) \rangle \underset{t \gg L_0^2/D}{=} 8 \frac{N}{L} \sqrt{\frac{Dt}{\pi}}. \quad (48)$$

At long times, everything happens as if the channel were infinitely short, as particles have diffused way further than the typical length of

the channel. Fluctuations thus are dominated by jumps between the left and right sides. At short times, however, fluctuations are dominated by particle exchanges from the channel to the reservoirs and vice versa—see dark gray in Fig. 7(a). They are similar in nature but contribute twice as less to the fluctuations, therefore explaining the scaling in Eq. (47). At intermediate times, fluctuations transit from one regime to the other.

Importantly, for channels, fractional noise is preserved. This is clear when one considers again the origin of fractional noise, as explored in Sec. II. In fact, fractional noise occurs when observing the statistics of random particles transiting from one region to another. For channels, where particles transit from reservoir to pore and pore to reservoir, one thus naturally expects to witness fractional noise. This highlights the universality of fractional noise.

2. Number of particles within the pore: "Charge carriers"

In the channel problem, we may also investigate the fluctuations of the number of particles $N_c(t)$ present inside the channel (with $-L_0/2 < x < L_0/2$). $N_c(t)$ is akin to the number of charge carriers (although here the particles are not charged), which is essential to understand ionic currents in nanoporous systems.¹⁶ The average number of particles in the channel is $\langle N_c(t) \rangle = \rho_0 L_0 \equiv N_0$. We can then write the fluctuations as

$$\langle N_c^2(t) \rangle = 2(1^2 p_{C \rightarrow R}(t) + 1^2 p_{L \rightarrow C}(t)), \quad (49)$$

where we abbreviated $\langle (N_c(t) - N_c(0))^2 \rangle = \langle N_c^2(t) \rangle$ and 1^2 highlights, as in Eq. (45), the contribution, e.g., +1 to N_c (1^2 to N_c^2), when a particle goes from the left to the center. We obtain

$$\langle N_c^2(t) \rangle = 2N_0 \left[\left(1 - e^{-\frac{L_0^2}{4Dt}} \right) \sqrt{\frac{4Dt}{\pi L_0^2}} + 1 - \operatorname{erf} \left(\frac{L_0}{\sqrt{4Dt}} \right) \right]. \quad (50)$$

This analytic result corresponds exactly with BD—see Fig. 8(d). The fluctuations of N_c feature two relevant limits. At early times, we find fractional noise

$$\langle N_c^2(t) \rangle \underset{t \ll L_0^2/D}{=} 4 \frac{N}{L} \sqrt{\frac{Dt}{\pi}}, \quad (51)$$

corresponding exactly to the early time regime for the number difference, Eq. (47). In fact, fluctuations of N_c are also dominated by particles in the vicinity of the pore mouth. At longer times, the fluctuations plateau,

$$\langle N_c^2(t) \rangle \underset{t \gg L_0^2/D}{=} 2N_0. \quad (52)$$

This is naturally expected, for the same reason as a plateau $2N$ is reached at long times for the number difference.

3. Spectrum of the number of particles within the pore

As fractional noise is also seen in the number of particles within the pore, we therefore expect its spectrum S_{N_c} to contain a signature of fractional noise as $1/f^{3/2}$. Such behavior is indeed observed for large enough frequencies—see Fig. 8(c). However, for low frequencies (long times), it is not straightforward to understand the noise spectrum dependence, as the fluctuations N_c saturate.

Based on the analysis of jumps mentioned above and following the method in Ref. 33, we can completely calculate the frequency spectrum. The correlation function of the number of particles within the pore simply corresponds to the probability that the particle did *not* leave the channel,

$$\langle N_c(t)N_c(0) \rangle = 1 - 2p_{C \rightarrow R}(t). \quad (53)$$

This can be simply evaluated as

$$\langle N_c(t)N_c(0) \rangle = N_0 \left[\left(e^{-\frac{t}{4D}} - 1 \right) \sqrt{\frac{Dt}{\pi L_0^2}} + \operatorname{erf}\left(\frac{L_0}{\sqrt{4Dt}}\right) \right]. \quad (54)$$

When the particles have diffused beyond the channel's extent ($t \gg L_0^2/D$), this correlation function decays as $1/\sqrt{t}$ and therefore continues to grow significantly when integrated over time (at least for times $t \ll L^2/D$). As a result, we may expect the spectrum at zero frequency to diverge as well—and not to saturate (as is seen, e.g., in Ref. 33). To infer the analytic expression for the spectrum, we write the Laplace transform of the correlation

$$\mathcal{L}[\langle N_c(t)N_c(0) \rangle](s) = -N_0 \frac{2\sqrt{D}}{L_0} \frac{1 - e^{-L_0\sqrt{s/D}}}{s^{3/2}}, \quad (55)$$

and simply

$$S_{N_c}(f) = \operatorname{Real}[\mathcal{L}[\langle N_c(t)N_c(0) \rangle](2i\pi f)]. \quad (56)$$

Analytic expansions of Eq. (56) show the expected frequency decay at high frequencies,

$$S_{N_c}(f) \underset{f \gg D/L_0^2}{=} \frac{2N\sqrt{2D}}{L} \frac{1}{(2\pi)^{3/2}} \frac{1}{f^{3/2}}. \quad (57)$$

At low frequencies, a decay as $1/f^{1/2}$ emerges

$$S_{N_c}(f) \underset{f \ll D/L_0^2}{=} N \frac{L_0^2}{\sqrt{2DL}} \frac{1}{(2\pi)^{1/2}} \frac{1}{f^{1/2}}. \quad (58)$$

Both decay laws are consistently obtained in BD simulations; see Fig. 8(c). Equation (58) is quite interesting as it shows the dramatic consequence of the slow decay in the correlation function on the noise spectrum. Overall, this demonstrates that low frequency noise is readily observed in our simple system for the number of particles within the pore. Brownian motion is thus sufficient to trigger intriguing noise features, with peculiar $1/f^\alpha$ dependence—without resorting to more complex effects.

At extremely small frequencies $f \ll D/L^2$, corresponding to very long times $t \gg L^2/D$, the particles feel the finite extent of the reservoirs, and one eventually finds a saturation of the frequency spectrum $S_{N_c}(f) = \frac{N}{8D} \frac{L_0^2}{L^2} \frac{1}{(1-L_0/L)^2}$. This saturation would be rarely observed in experiments as it would require acquisitions over days (taking, e.g., $L = 1$ cm and $D = 2 \times 10^{-9}$ m²/s) and therefore is not relevant, in general. Note that this saturation is not comparable to the saturation observed in Ref. 33, which examines infinite reservoirs.

When considering realistic geometries, with a thick membrane, we may therefore expect different noise regimes according to the relative values of the pore width (radius, or typical cross section size)

and the pore length. Section IV B is dedicated to summarizing the scalings and transitions between behaviors in the general nanochannel geometry, with a focus on the number of particles within the pore.

B. General geometry and consequences for charge carrier fluctuations

1. Mapping to a rates problem and limit regimes

Similarly, as for the narrow problem, we can map the nanochannel problem to a rates problem—see Fig. 7(b). We use similar notations and take $p(x, t)$ and $q(x, t)$ as the probability that a particle is in the passing or blocked state at position x and time t . Compared to the short pores in Sec. III, here, over the channel length L_0 , the blocked state does not exist; the passing state does not exchange with the blocked state. As in Sec. III, we can solve for the probability distribution functions p and q in Laplace space and then calculate the fluctuations of ΔN and N_c using a similar formalism as for Eq. (45). Full solutions are detailed in Appendix D.

The results (both analytic and of BD simulations) point, as expected, to an interplay of channel-like behavior at short times, as seen in Sec. IV A, and pore-like behavior at longer times, as in Sec. III. We can distinguish five phases (considering pores that are at least as long as they are wide $L_0 \gtrsim R$):

- [initial, dark gray in Fig. 7(a)] For $t \ll t_{\text{early}} = \frac{R^2}{D}$, fractional noise [$\langle \Delta N(t)^2 \rangle = \langle N_c(t)^2 \rangle = 4c_0 \mathcal{G}_{\mathcal{R}} \sqrt{Dt}$], where $\mathcal{G}_{\mathcal{R}}$ is a geometric prefactor taking into account the details of the channel geometry and c_0 is the average particle concentration.
- [early, light blue in Fig. 7(a)] For $t_{\text{early}} \ll t \ll t_{\text{channel}} = L_0^2/D$, fractional noise with twice as large amplitude [$\langle \Delta N(t)^2 \rangle = \langle N_c(t)^2 \rangle = 8c_0 \mathcal{G}_{\mathcal{R}} \sqrt{Dt}$]
- [intermediate, purple in Fig. 7(a)] For $t_{\text{channel}} \ll t \ll t_{\text{int}} \simeq \frac{L_m^4}{R^4} R^2/D$, diffusive noise in the number difference, saturation for N_c .
- [later, gray in Fig. 7(a)] For $t_{\text{int}} \ll t \ll t_{\text{late}} \simeq \frac{L^2}{D}$, fractional noise in the number difference [$\langle \Delta N(t)^2 \rangle = 8\rho_0 \sqrt{Dt}$], saturation for N_c .
- [final] For $t \gg t_{\text{late}}$, saturation for all variables.

Full derivations and agreement of BD simulations with analytic results showing the interplay of these five regimes are reported in Appendix D (Figs. 11 and 12). We now turn to the investigation of the noise spectrum.

2. Spectrum of the number of particles within the pore

a. *Noise spectrum.* Following a similar approach as in Sec. IV A, we find the Laplace transform of the correlation function

$$\begin{aligned} \mathcal{L}[\langle N_c(t)N_c(0) \rangle](s) = & -N_0 \frac{4\sqrt{D}}{L_0} \frac{1}{s^{3/2}} (1 - e^{-qL_0}) \\ & \times \frac{\tilde{q}(q_{\text{on}} + q_{\text{off}})}{e^{-qL_0} q_{\text{off}}(\tilde{q} - q) + q q_{\text{off}} + (q_{\text{off}} + 2q_{\text{on}})\tilde{q}}, \end{aligned} \quad (59)$$

where we recall that $q = \sqrt{s/D}$ and $\tilde{q} = \sqrt{q^2 + (q_{\text{on}} + q_{\text{off}})/D}$. Here, $N_0 = \langle N_c(t) \rangle = c_0 \pi R^2 L_0$ is the average number of particles within the pore and c_0 is the particle concentration. Using Eq. (56), we can fully

obtain the spectrum of fluctuations for N_c that agrees remarkably with BD simulations—see Fig. 9.

Expanding Eq. (59), it is possible to obtain limiting relevant regimes for the fluctuation spectrum. Here, we assume that the channel is rather isolated on the membrane $L_m \gtrsim L_0$ (corresponding to $q_{\text{on}} \ll D/L_0^2$) such that three characteristic behaviors emerge in the fluctuation spectrum:

- at very low frequencies, the $1/f^{1/2}$ decay is observed,

$$S_{N_c}(f) \underset{f \ll q_{\text{on}}}{=} \frac{q_{\text{on}}}{q_{\text{on}} + q_{\text{off}}} N_0 \frac{L_0}{\sqrt{2D}} \frac{1}{(2\pi)^{1/2}} \frac{1}{f^{1/2}}, \quad (60)$$

which is exactly Eq. (58) multiplied by a geometric prefactor $\frac{q_{\text{on}}}{q_{\text{on}} + q_{\text{off}}} = \frac{\pi R^2}{4L_m^2}$ corresponding to the open pore area (for a circular pore of radius R). As mentioned earlier, this regime is not seen in theoretical derivations of Ref. 33. In fact, Ref. 33 assumes an infinitely small pore on a membrane, giving $q_{\text{on}} \rightarrow 0$, and hence, the $1/f^{1/2}$ regime does not appear.

- At intermediate frequencies, we find a plateau

$$S_{N_c}(f) \underset{q_{\text{on}} \ll f \ll L_0^2/D}{=} \frac{2}{3} N_0 \frac{L_0^2}{D} \left(1 + \frac{6}{L_0} \sqrt{\frac{D}{q_{\text{off}}}}\right). \quad (61)$$

This (temporary) saturation corresponds to intermediate times where no significant exchange with the reservoirs is possible yet. Equation (15) of Ref. 33 also predicts a saturation for the circular pore $S_{N_c}(f) = \frac{1}{3} N_0 \frac{L_0^2}{D} \left(1 + \frac{3\pi}{2} \frac{R}{L_0}\right)$, while we find $S_{N_c}(f) = \frac{2}{3} N_0 \frac{L_0^2}{D} \left(1 + \frac{3}{\sqrt{\pi}} \frac{R}{L_0}\right)$. These slight differences originate from the approximate model for reservoirs in Ref. 33.

- At high frequencies, we recover the $1/f^{3/2}$ decay,

$$S_{\Delta N}(f) \underset{f \gg D/L_0^2}{=} \frac{2N_0}{L_0} \sqrt{2D} \frac{1}{(2\pi)^{3/2}} \frac{1}{f^{3/2}}. \quad (62)$$

This decay corresponds exactly to that observed in infinitely long channels Eq. (57). Reference 33 predicts a similar regime for small pores (with an amplitude twice as large) yet only at intermediate frequencies ($f \ll D/R^2$). At large frequencies, Ref. 33 finds a decay as $1/f^2$. These differences originate from the approximate model for reservoirs in Ref. 33. A graphical comparison with Ref. 33 is reported in Appendix D (Fig. 13).

In contrast with very long channels, *actual* channels feature a plateau in the frequency spectrum. The extent of this plateau in the frequency spectrum is longer if the channel is more narrow. For example, the onset of the $1/f^{1/2}$ regime occurs at much smaller frequencies for the long channel of Fig. 9(b) than for the short channel of Fig. 9(a) [hence, it is not seen in Fig. 9(b)]. Other numerical setups also observe the emergence of such a plateau.³⁵

b. Optimizing signal-to-noise ratio We now discuss how our results can be harnessed to optimize the signal-to-noise ratio for currents related to the number of particles within the pore. Similarly, as in Sec. III, if an external field E is applied, we expect to measure an average particle current scaling as $\langle I_{\text{ext}} \rangle = \langle \mathcal{G} \rangle E$, where \mathcal{G} is the pore's conductance. Yet, conductance (at large enough concentrations, for electric fields) is proportional to the number of charge carriers.¹⁶ Although our particles are uncharged, we expect that, e.g., for strong electrolytes and systems where charge effects are not predominant, the results uncovered for uncharged particles would translate for charged species. We therefore use N_c as a representative for the number of charge carriers,

$$\frac{\langle \delta I_{\text{ext}} \rangle}{\langle I_{\text{ext}} \rangle^2} = \frac{\langle \delta G^2 \rangle}{\langle G \rangle^2} = \frac{\langle N_c^2 \rangle}{N_0^2} \sim \begin{cases} 1/c_0 L_m^2 & \text{for } f \ll q_{\text{on}} \\ L_0^2/N_0 & \text{for } q_{\text{on}} \ll f \ll D/L_0^2 \\ 1/N_0 & \text{for } f \gg D/L_0^2. \end{cases} \quad (63)$$

The signal-to-noise ratio can thus be maximized working at high concentrations (large c_0 and N_0) in quite short pores (L_0). Narrow pores (small R) decrease the signal-to-noise ratio (by decreasing N_0), and therefore, short pores are preferred in this setting where noise originates from purely diffusive mechanisms.

V. CONCLUSIONS AND DISCUSSION

A. Emergence of fractional noise in nanoporous systems

Fractional noise originates from particle exchanges between one region and another. In nanoporous systems, such exchanges are ubiquitous as solute particles go from the reservoir to pore and pore to reservoir. As a consequence, fractional noise emerges naturally in nanoporous systems. It yields fluctuations in time scaling as \sqrt{t} and traces in the low frequency noise spectrum decaying as $1/f^{3/2}$. We have demonstrated the presence of such low frequency traces in various pore geometries. Brownian motion is thus already a key

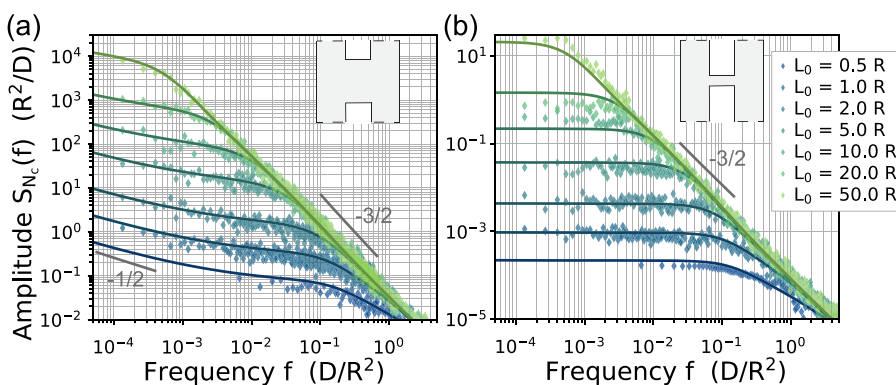


FIG. 9. Noise on the number of particles within the pore in various pores. Noise spectrum of N_c for (a) broad pores with $R = 0.4L_m$ and (b) narrow pores with $R = 0.02L_m$ for different pore lengths as indicated in the shared legend. Dots are results from BD simulations. Here, the pore is square with side $2R$. Full lines correspond to the analytic result of Eq. (59). Other simulation parameters correspond to that of Fig. 1.

ingredient to trigger such low frequency noise—without resorting to more complex effects.

Such $1/f^{3/2}$ dependence in the noise spectrum has been consistently seen in many different settings—though never rationalized as a generic feature inheriting from fractional noise. In artificial systems, $1/f^{3/2}$ has been measured¹⁷ and also $1/f^2$ in narrow pores.^{1,2} In more advanced numerical systems (including adsorption in the inner pore as compared to our simulations), $1/f^{3/2}$ dependencies have been seen in the number of particles present within the pore.³⁵ In approximate theoretical models, $1/f^{3/2}$ and $1/f^2$ have been consistently seen as well.^{22,33,41} These results point to the fact that fractional noise decaying as $1/f^\alpha$ with $\alpha = 1.5$ – 2 prevails in real systems and indeed has consequences even when more complex effects are at play.

We also discussed a $1/f^{1/2}$ dependence in the noise spectrum for the number of particles within the pore (akin to the number of charge carriers for charged particles), appearing for frequencies $f \ll L_m^2/D$. Similarly, low frequency noise decaying as $1/f^\alpha$ with $\alpha \approx 0.5$ has also been observed in a few experimental or numerical systems.^{11,35} However, it is harder to speculate that fractional noise is the origin of such measurements. In fact, it involves very low frequencies, either not attainable experimentally or were a number of other processes may very well be at play (such as adsorption/desorption.³⁵)

The effect of reservoirs can be reduced to a one-dimensional rates problem. In this work, we have introduced a method to map a complex 3D geometry with reservoirs and pores to a simple 1D geometry (or more precisely $2 \times 1D$). This mapping relies on transition rates from the passing to the blocked lines and vice versa. These rates are established from detailed balance equilibrium and do not rely on any additional assumption. Remarkably, such a mapping allows us to reproduce with perfect accuracy the results of 3D simulations. It also opens perspectives to drastically simplify numerical simulations (by simulating particles on 1D lines instead of 3D reservoirs) and analytic calculations.

Note that this is in sharp contrast with other theoretical investigations, which rely either on approximate entrance and exit rates in the pore^{33,41} or on approached, simplified geometries.³⁵ It also allows us to probe efficiently the effect of different pore geometries.⁴⁷

The mapping has great potential to reduce the cost of simulating large reservoirs and probe further effects on nanoporous transport. For example, the mapping could easily be extended to the investigation of more varied geometries, adsorption within the pore,³⁵ or equilibrium reactions at boundaries mimicking electrodes. Its applicability to other systems remains to be assessed. For example, when charges are added, and electric fields may affect the motion of ions significantly between regions, such a mapping may have to be adapted.

B. Further discussion

In essence, fractional noise is expected to occur in many systems beyond nanoporous transport. For example, such fractional noise or $1/f^{3/2}$ has been observed in the context of electrochemistry at surfaces.^{48,49} Furthermore, fractional Brownian walks have been used to model or explain subdiffusion patterns for molecules such as mRNA or other large molecules evolving in crowded environments such as cells^{50,51} or with adsorption to surfaces.⁵² It remains

to be assessed whether such fractional behavior originates from the same physical principles (namely, particles transitioning between one region and another) or from other mechanisms.

Interestingly, our study also shows how crucial the parameters of the experimental measurement may affect observation. For example, fitting of the low frequency noise over only a few decades may lead to a variety of decay exponents [as is observed in Fig. 5(b)]. Furthermore, currents depending on the acquisition frequency may experience more or less noise. Acquisition frequency dependency of nanopore conductance has been measured in specific cases.⁵³

Beyond this equilibrium context, it remains to be assessed how fractional noise survives out-of-equilibrium. For example, we can expect the probability of events where particles exchange back and forth from the pore to the reservoir to decay with an applied external field. This may result in a non-linear dependence of the noise with the applied external field. To some extent this is reminiscent—although implying a different mechanism—of other non-linearities depending on the applied field, for example, in conductivity measurements of charged solutions.⁵⁴

ACKNOWLEDGMENTS

S.M. is indebted to Aleksandar Donev for acute scientific advice and numerous discussions. S.M. recognizes the help of Michel Pain, who pointed to relevant references in the pure math literature associated with this problem. S.M. is further thankful to Alejandro L. Garcia, Amaury Hayat, Miranda Holmes-Cerfon and Benjamin Rotenberg for fruitful discussions. S.M. was supported, in part, by the MRSEC Program of the National Science Foundation under Award No. DMR-1420073. S.M. acknowledges funding from a Marie Skłodowska Curie fellowship under Award No. 839225—MolecularControl project.

APPENDIX A: NUMERICAL METHODS

1. Brownian dynamics simulations

Brownian dynamics of particles translocating through pores are implemented using a custom made Python routine.

a. System parameters

The simulation is performed in non-dimensional time and length scales. The length scale of reference is set to be the pore size R and the time scale of reference $\frac{R^2}{D}$. In general, the time step was taken to be $\Delta t = 0.05 \frac{R^2}{D}$ and is much smaller compared to the smallest time scale of the system $\frac{R^2}{D}$. In general, $N = 1000$ particles were simulated over 3×10^7 time steps. Other system parameters (such as box size L and membrane size L_m) are always specified in figure captions where the relevant data are shown.

In systems made of particles on a line, where no pore size is defined, we use ℓ as the unit length and ℓ^2/D as the unit time.

b. Dynamics

The noise generation is done through Python's numpy random number generator. At each time step, for each particle, a random number with standard normal distribution (`numpy.random.randn`) is generated and the particle's position is updated via Eq. (1). For each independent simulation, the seed is set to a different value.

Reflections on the reservoir walls and on the membrane are implemented using De Michele's algorithm.⁵⁵ All measured quantities were thoroughly checked to be independent of simulation parameters. In particular, they were checked to be independent of the time step Δt .

We stress that the particles are intended to be the most simple Brownian walkers. They are non-interacting and point-like particles.

2. Partial differential equation solvers

To solve numerically the rates problem defined by Eq. (25), a standard forward Euler scheme was implemented in a custom made Python routine. The numerical solutions were independent of the chosen time and space step. In general, the time step used was $\Delta t = 0.05 - 0.005 \frac{R^2}{D}$ (increasing to larger values after smoothing out of the initial step functions) and space step $\Delta x = L/(N_x - 1)$, with $N_x = 2000$. With $L = 500R$ in general, this gives $\Delta x = 0.25R$, and therefore, $\Delta t \ll \Delta x^2/D$ is always verified, ensuring the stability of the forward Euler scheme.

APPENDIX B: SOLVING THE RATES PROBLEM

To solve the rates problem defined by Eq. (25), we focus on the eigenvectors of the partial differential equation system

$$\begin{cases} z_1 = p + q, \\ z_2 = q_{\text{off}}p - q_{\text{on}}q \end{cases} \quad (\text{B1})$$

that obey an uncoupled system of equations

$$\begin{cases} \partial_t z_1 = D \partial_{xx} z_1, \\ \partial_t z_2 = -(q_{\text{off}} + q_{\text{on}})z_2 + D \partial_{xx} z_2, \\ \partial_x z_1|_{x=\pm L/2} = \partial_x z_2|_{x=\pm L/2} = 0. \end{cases} \quad (\text{B2})$$

To specify the boundary conditions, we write $z_i^L = z_i(x \leq 0)$ and $z_i^R = z_i(x \geq 0)$ the left of the wall and right of the wall components of the eigenvectors. They verify that

$$\begin{cases} \partial_x z_1^L(0, t) = \partial_x z_1^R(0, t), \\ \partial_x z_2^L(0, t) = \partial_x z_2^R(0, t), \\ z_1^L(0, t)q_{\text{on}} + z_2^L(0, t) = z_1^R(0, t)q_{\text{on}} + z_2^R(0, t), \\ \partial_x z_1^L(0, t)q_{\text{off}} = \partial_x z_2^L(0, t), \end{cases} \quad (\text{B3})$$

and z_1 and z_2 are both discontinuous in 0. The initial conditions verify that

$$\begin{cases} z_2^L(x < 0, 0) = z_2(x > 0, 0) = 0, \\ z_2^L(0, 0) = q_{\text{off}}p_0/2 - q_{\text{on}}p_0 \frac{q_{\text{off}}}{q_{\text{on}}} = -q_{\text{off}}p_0/2, \\ z_2^R(x = 0, 0) = -z_2^L(0, 0) = q_{\text{off}}p_0/2, \\ z_1^L(x < 0, 0) = p_0 \frac{q_{\text{on}} + q_{\text{off}}}{q_{\text{on}}}, \\ z_1^L(x > 0, 0) = 0, \\ z_1^L(x = 0, 0) = p_0/2 + p_0 \frac{q_{\text{off}}}{q_{\text{on}}} = p_0 \frac{q_{\text{on}} + 2q_{\text{off}}}{2q_{\text{on}}}, \\ z_1^R(x = 0, 0) = p_0/2 + 0 = z_1^L(x = 0, 0) - 2p_0 \frac{q_{\text{off}}}{2q_{\text{on}}}. \end{cases} \quad (\text{B4})$$

Importantly, this set of equations and boundary conditions is compatible with a wrapping

$$\begin{cases} z_2^R(x) = \tilde{z}_2(x), \\ z_2^L(-x) = -\tilde{z}_2(x), \\ z_1^R(x) = \tilde{z}_1(x), \\ z_1^L(-x) = 2z_0 - \tilde{z}_1(-x), \end{cases} \quad (\text{B5})$$

where $z_0 = p_0 \frac{q_{\text{on}} + q_{\text{off}}}{2q_{\text{on}}}$, \tilde{z}_i need only to be defined on a half space, and the boundary conditions are

$$\begin{cases} \tilde{z}_1(x > 0, 0) = 0, \tilde{z}_1(x = 0, 0) = p_0/2, \\ \tilde{z}_2(x > 0, 0) = 0, \tilde{z}_2(x = 0, 0) = q_{\text{off}}p_0/2, \\ (z_0 - \tilde{z}_1(0, t))q_{\text{on}} = \tilde{z}_2(0, t), \\ \partial_x \tilde{z}_1(0, t)q_{\text{off}} = \partial_x \tilde{z}_2(0, t). \end{cases} \quad (\text{B6})$$

These boundary conditions are well suited for solving the problem in Laplace space. We define the Laplace transform

$$\hat{z}_i(x, s) = \int_0^\infty e^{-st} \tilde{z}_i(x, t) dt, \quad (\text{B7})$$

where we use here for compactness the notation \hat{z} for the Laplace transform instead of $\mathcal{L}[z]$. The general solution to the system of equations is

$$\hat{z}_i = A_i e^{q_1 x} + B_i e^{-q_1 x}, \quad (\text{B8})$$

where $q_1 = q = \sqrt{\frac{s}{D}}$ and $q_2 = \tilde{q} = \sqrt{q^2 + \frac{q_{\text{off}} + q_{\text{on}}}{D}}$. In addition, the integration constants A_i, B_i are determined by the boundary conditions and obey the following set of equations:

$$\begin{cases} A_1 e^{qL/2} - B_1 e^{-qL/2} = 0, \\ A_2 e^{\tilde{q}L/2} - B_2 e^{-\tilde{q}L/2} = 0, \\ (z_0 \frac{1}{s} - A_1 - B_1)q_{\text{on}} = A_2 + B_2, \\ (A_1 - B_1)q q_{\text{off}} = (A_2 - B_2)\tilde{q}. \end{cases} \quad (\text{B9})$$

We recall that

$$\langle \Delta N^2(t) \rangle = 4N \int_0^{L/2} [p(x, t) + q(x, t)] dx \quad (\text{B10})$$

such that

$$\begin{aligned} \partial_t \langle \Delta N^2(t) \rangle &= 4N \int_0^{L/2} \partial_t [p(x, t) + q(x, t)] dx \\ &= 4N \int_0^{L/2} D \partial_{xx} [p(x, t) + q(x, t)] dx \\ &= -4N D \partial_x [p(x, t) + q(x, t)]_{x=0} \\ &= -4N D \partial_x [z_1^R]_{x=0}. \end{aligned} \quad (\text{B11})$$

We can thus obtain in Laplace space

$$\langle \Delta \hat{N}^2(t) \rangle = -\frac{4N}{q} (A_1 - B_1). \quad (\text{B12})$$

The resulting $\langle \Delta \hat{N}^2(t) \rangle$ is

$$\langle \Delta \hat{N}^2(t) \rangle = 8N z_0 \frac{\sqrt{D}}{s^{3/2}} \frac{q_{\text{on}}}{q_{\text{off}} \frac{q}{\tilde{q}} \coth(\tilde{q}L/2) + q_{\text{on}} \coth(qL/2)} \quad (\text{B13})$$

for which no analytic real time expression exists.

1. Analytic result at long times

Fluctuations at long times in Laplace space correspond to small values of s . We find for the asymptotic behavior

$$\langle \Delta \hat{N}^2(t) \rangle_{s \rightarrow 0} = 4N z_0 \frac{\sqrt{D}}{s^{3/2}} qL = 4N z_0 L \frac{1}{s}, \quad (\text{B14})$$

translating to real time and making use of the expression of z_0 , and we obtain

$$\langle \Delta N^2(t) \rangle_{t \rightarrow \infty} = 2N, \quad (\text{B15})$$

which is exactly what is expected.

APPENDIX C: DATA FOR THE SQUARE PORE

For a square pore of side $2R$, we use the phenomenological rates

$$q_{\text{off}}^{-1} = \frac{(2R)^2}{4D} \quad \text{and} \quad q_{\text{on}}^{-1} = \frac{4L_m^2 - (2R)^2}{4D}. \quad (\text{C1})$$

In Fig. 10, we present the fluctuations $\langle \Delta N(t)^2 \rangle$ with time using the rates model with this phenomenological choice and performing BD simulations through a square pore. The model and numerical data are in perfect agreement.

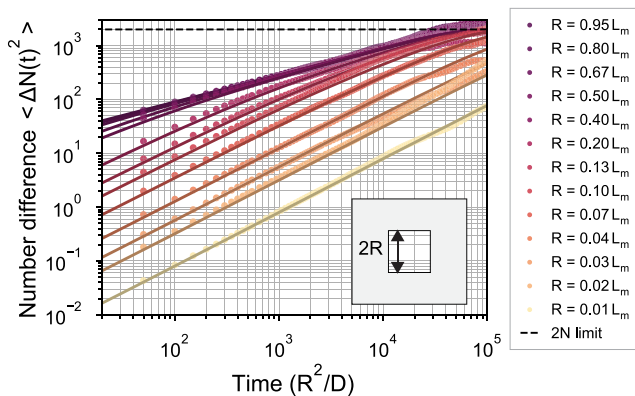


FIG. 10. The rates model reproduces the regimes observed in a 3D square pore. Number difference fluctuations with time for several values of R/L_m as indicated with the various colors. Dots correspond to data from BD simulations, and lines correspond to the analytic solutions of Eq. (25). Other numerical parameters correspond to that of Fig 5(b).

APPENDIX D: SOLVING THE NANOCANNEL PROBLEM

1. Rates problem in the nanochannel geometry

We use similar notations and take $p(x, t)$ and $q(x, t)$ as the probability that a particle is in the passing or blocked state, respectively, at position x and time t . Those quantities obey the following coupled set of equations:

$$\begin{cases} \text{for } |x| > L_0/2, & \begin{cases} \partial_t p = -q_{\text{off}} p + q_{\text{on}} q + D \partial_{xx} p, \\ \partial_t q = +q_{\text{off}} p - q_{\text{on}} q + D \partial_{xx} q, \end{cases} \\ \text{for } |x| \leq L_0/2, & \partial_t p = D \partial_{xx} p, \\ \partial_x q|_{x=\pm L_0/2} = 0 & \partial_x p|_{x=\pm L_0/2} = \partial_x q|_{x=\pm L_0/2} = 0, \end{cases} \quad (\text{D1})$$

and q is not defined for $-L_0 < 2x < L_0$. p and $\partial_x p$, however, are continuous over the whole domain, especially in $x = \pm L_0/2$. To calculate the fluctuations of ΔN , we must proceed as mentioned above and consider several jumps, starting from either the left-hand side or the channel itself. Here, we report as an example the initial conditions for the particle starting on the left (taking the initial values corresponding to the probabilities to find the particle on the left at equilibrium),

$$\begin{cases} p(x < -L_0/2, t = 0) = \frac{\pi R^2}{\mathcal{V}} = p_0, \\ q(x < -L_0/2, t = 0) = \frac{(4L_m^2 - \pi R^2)}{\mathcal{V}} = p_0 \frac{q_{\text{off}}}{q_{\text{on}}}, \\ p(x > -L_0/2, t = 0) = q(x > -L_0/2, t = 0) = 0. \end{cases} \quad (\text{D2})$$

Here, $\mathcal{V} = 4L_m^2(L - L_0) + L_0\pi R^2$ is the total accessible volume. Similarly, as in the very long nanochannel problem, we now have to distinguish between particles that actually went to the other side and particles that only made it inside the channel. The probability that the particle made it to the other side at time t is

$$p_{L \rightarrow R}(t) = \int_{L_0/2}^{L/2} [p(x, t) + q(x, t)] dx, \quad (\text{D3})$$

and the probability that it went inside the channel is

$$p_{L \rightarrow C}(t) = \int_0^{L_0/2} p(x, t) dx. \quad (\text{D4})$$

A similar formalism applies for particles starting inside the channel.

2. Solving the rates problem

To solve the rates problem defined by Eq. (D1), we adopt a similar method as in Appendix B and focus on the eigenvectors of the partial differential equation system. Beyond the channel, for $|x| > L_0/2$, we take

$$\begin{cases} z_1 = p + q, \\ z_2 = q_{\text{off}} p - q_{\text{on}} q, \end{cases} \quad (\text{D5})$$

and inside the channel, we simply take

$$z_m = p \quad (\text{D6})$$

that obey an uncoupled system of equations

$$\begin{cases} \partial_t z_1 = D\partial_{xx}z_1 \text{ for } |x| > L_0/2, \\ \partial_t z_m = D\partial_{xx}z_m \text{ for } |x| \leq L_0/2, \\ \partial_t z_2 = -(q_{\text{off}} + q_{\text{on}})z_2 + D\partial_{xx}z_2 \text{ for } |x| > L_0/2, \\ \partial_x z_1|_{x=\pm L_0/2} = \partial_x z_2|_{x=\pm L_0/2} = 0. \end{cases} \quad (\text{D7})$$

To specify the remaining boundary conditions, we split the domain and write $z_i^L = z_i(x \leq 0)$ and $z_i^R = z_i(x \geq 0)$ the components of the eigenvectors to the left and right of $x = 0$. The boundary conditions can be derived with minimal algebra,

$$\begin{cases} \partial_x q|_{x=\pm L_0/2} = 0 \Leftrightarrow q_{\text{off}}z_1^{L/R}|_{x=\pm L_0/2} = z_2^{L/R}|_{x=\pm L_0/2}, \\ \text{continuity of } p \Leftrightarrow \frac{q_{\text{on}}z_1^{L/R} + z_2^{L/R}}{q_{\text{off}} + q_{\text{on}}}\Big|_{x=\pm L_0/2} = z_m^{L/R}|_{x=\pm L_0/2}, \\ \text{continuity of } \partial_x p \Leftrightarrow \partial_x \frac{q_{\text{on}}z_1^{L/R} + z_2^{L/R}}{q_{\text{off}} + q_{\text{on}}}\Big|_{x=\pm L_0/2} = \partial_x z_m^{L/R}|_{x=\pm L_0/2}. \end{cases} \quad (\text{D8})$$

a. Starting from the left

We now define the Laplace transforms

$$\tilde{z}_i^{L/R}(x, s) = \int_0^\infty e^{-st} (z_i^{L/R}(x, t) - z_i^{L/R}(x, t=0)) dt. \quad (\text{D9})$$

Note that here the Laplace transforms are taken with respect to the base value. The general solutions of the partial differential functions aforementioned are

$$\tilde{z}_i^{L/R} = A_i^{L/R} e^{q_1 x} + B_i^{L/R} e^{-q_1 x}, \quad (\text{D10})$$

where $q_1 = q_m = q = \sqrt{\frac{s}{D}}$ and $q_2 = \tilde{q} = \sqrt{q^2 + \frac{q_{\text{off}} + q_{\text{on}}}{D}}$. In addition, the integration constants A_i, B_i are determined by the boundary conditions Eq. (D8). We recall that the contributions to the noise from this first situation are

$$\langle \Delta N^2(t) \rangle^{(1)} = 8N \int_{L_0/2}^{L/2} [p(x, t) + q(x, t)] dx + 2N \int_{-L_0/2}^{L_0/2} p(x, t) dx \quad (\text{D11})$$

such that

$$\begin{aligned} \partial_t \langle \Delta N^2(t) \rangle^{(1)} &= 8N \int_{L_0/2}^{L/2} \partial_t z_1^R dx + 2N \int_{-L_0/2}^{L_0/2} \partial_t z_m dx \\ &= 8N \int_{L_0/2}^{L/2} D\partial_{xx}z_1^R dx + 2N \int_{-L_0/2}^{L_0/2} D\partial_{xx}z_m dx \\ &= -8N D\partial_x [z_1]_{x=L_0/2} + 2N D\partial_x [z_m]_{x=L_0/2} \\ &\quad - 2N D\partial_x [z_m]_{x=0}. \end{aligned} \quad (\text{D12})$$

We thus obtain in Laplace space

$$\begin{aligned} \langle \hat{\Delta N}^2(s) \rangle^{(1)} &= 8 \frac{N}{q} (B_1^R e^{-qL_0/2} - A_1^R e^{qL_0/2}) \\ &\quad + 2 \frac{N}{q} (A_m e^{-qL_0/2} - B_m e^{qL_0/2}) \\ &\quad - A_m e^{qL_0/2} + B_m e^{qL_0/2}. \end{aligned} \quad (\text{D13})$$

Starting from the left side, $z_1^L(t=0) = \frac{1}{L} \frac{1}{1 - \frac{L_0}{L} (\frac{1}{1+r})}$, where $r = q_{\text{on}}/q_{\text{off}}$, and otherwise initial conditions are 0.

b. Starting from the channel

We can solve in a similar way for particles starting from the center of the domain. In that case, the problem is symmetric with respect to the center $x = 0$ and can be simplified accordingly. Using similar notations, we obtain

$$\partial_t \langle \Delta N^2(t) \rangle^{(2)} = 2N \int_{L_0/2}^{L/2} \partial_t z_1^R dx, \quad (\text{D14})$$

and in Laplace space,

$$\langle \hat{\Delta N}^2(s) \rangle^{(2)} = 2 \frac{N}{q} (B_1^R e^{-qL_0/2} - A_1^R e^{qL_0/2}). \quad (\text{D15})$$

Starting from the channel, the base conditions are 0 everywhere except for $z_m(t=0) = \frac{r}{1+r} \frac{1}{L} \frac{1}{1 - \frac{L_0}{L} (\frac{1}{1+r})}$.

The total fluctuations sum up to

$$\langle \hat{\Delta N}^2(t) \rangle = \langle \hat{\Delta N}^2(t) \rangle^{(1)} + \langle \hat{\Delta N}^2(t) \rangle^{(2)}. \quad (\text{D16})$$

c. Correlations of the number of particles within the channel

The spectrum of the correlation function of the number of particles within the channel can be simply inferred starting from

$$\langle N_c(t) N_c(0) \rangle = 2 \int_0^{L_0/2} z_m(x, t) dx, \quad (\text{D17})$$

and going to Laplace space, we simply obtain

$$\mathcal{L}[\langle N_c(t) N_c(0) \rangle](s) = -2 \frac{D}{s} \partial_x z_m \Big|_{x=L_0/2}. \quad (\text{D18})$$

3. Solutions in Laplace space

Here, we report only the results when formally $L \rightarrow \infty$, corresponding to times $t \ll L^2/D$. This imposes $A_{1/2}^{R/L} = 0$ and therefore simplifies greatly the problem leaving only six integration constants to be found. We write $r = q_{\text{on}}/q_{\text{off}}$ and $r(s) = q/\tilde{q}$ such that

$$\begin{aligned} \langle \hat{\Delta N}^2(s) \rangle &= 4N \frac{\sqrt{D}}{s^{3/2}L} r(1+r)(1+e^{L_0q}) / ([1+r - L_0/L] \\ &\quad \times [r(q) - 1 + e^{L_0q}(r(q) + 1 + 2r)]). \end{aligned} \quad (\text{D19})$$

Similarly,

$$\begin{aligned} \langle \hat{N}_c^2(s) \rangle &= 4N \frac{\sqrt{D}}{s^{3/2}L} r(1+r)(-1+e^{L_0q}) / ([1+r - L_0/L] \\ &\quad \times [1 - r(q) + e^{L_0q}(r(q) + 1 + 2r)]). \end{aligned} \quad (\text{D20})$$

These solutions recover, in particular, the expected limits for infinitely thin pores $L_0 = 0$ and infinitely long channels $q_{\text{off}} = 0$. Agreement of these analytic results with BD simulations is reported in Figs. 11 and 12.

4. Limit regimes

a. Narrow pores

We start by investigating the limit regimes in narrow pores ($r \rightarrow 0$). We obtain

$$\langle \Delta \hat{N}^2(s) \rangle = 4N \frac{\sqrt{D}}{s^{3/2}L} r(1 + e^{L_0 q}) / ([1 - L_0/L] \times [r(q) - 1 + e^{L_0 q}(r(q) + 1)]) \quad (\text{D21})$$

that is easily amenable to early/intermediate/late time investigation. We start by short times, corresponding to $s, q \rightarrow \infty$. We find that

$$\langle \Delta \hat{N}^2(s) \rangle = 2N \frac{\sqrt{D}}{s^{3/2}} \frac{r}{L - L_0} \quad (\text{D22})$$

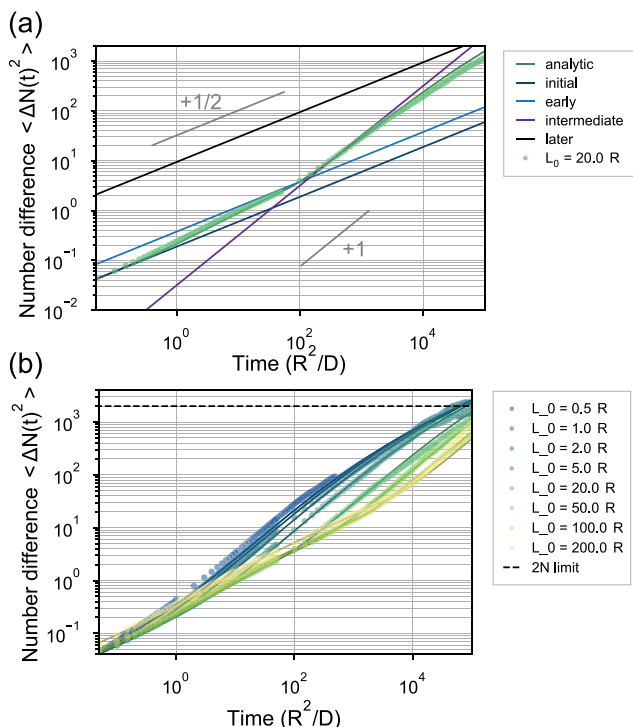


FIG. 11. The rates model reproduces the regimes for the number difference fluctuations observed in a long 3D square pore. Here, $R = 0.2L_m$, but similar results were also found for much small pores. (a) Different regimes with time, as illustrated in Fig. 7(a), for a specific channel geometry. Initial corresponds to Eq. (D23), early corresponds to Eq. (D26), intermediate corresponds to Eq. (D32), and later corresponds to Eq. (D33). The later regime is not so much observed as it corresponds to a time point where fluctuations reach the saturation limit $2N$. (b) Number difference fluctuations with time for several values of L_0/R as indicated with the various colors. Dots correspond to data from BD, and lines correspond to the analytic solutions Eq. (D19). Numerical parameters correspond to that of Fig. 1.

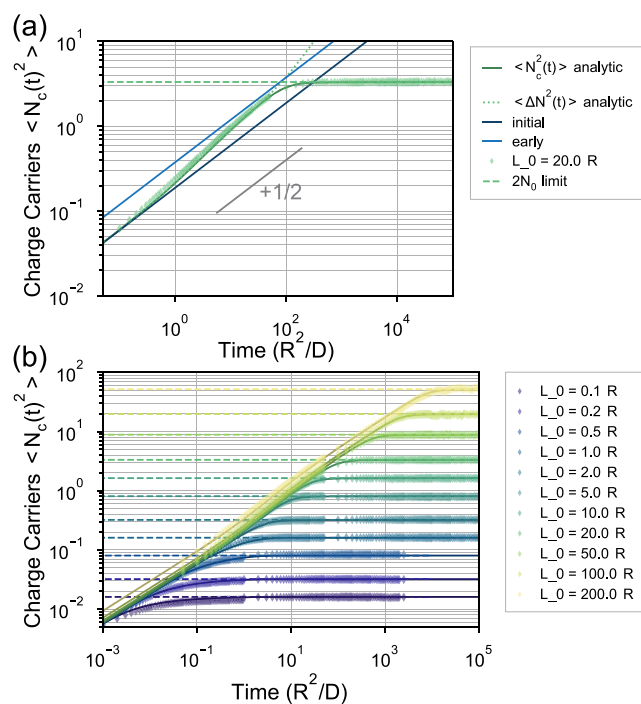


FIG. 12. The rates model reproduces the regimes for the number of particles within the pore fluctuations observed in a long 3D square pore. Here, $R = 0.2L_m$, but similar results were also found for much small pores. (a) Different regimes with time, as illustrated in Fig. 7(a), for a specific channel geometry. Initial corresponds to Eq. (D24), early corresponds to Eq. (D27), and saturation corresponds to the $2N_0$ limit of Eq. (D29). Analytic solutions for $\langle N_c^2(t) \rangle$ and $\langle \Delta N^2(t) \rangle$ overlap at short times. (b) Number difference fluctuations with time for several values of L_0/R as indicated with the various colors. Dots correspond to data from BD, and lines correspond to the analytic solutions Eq. (D20). Numerical parameters correspond to that of Fig. 1.

such that the real time evolutions scale as

$$\langle \Delta N^2(t) \rangle_{t \ll L_0^2/D} = 4 \frac{N}{L - L_0} \frac{\pi R^2}{4L_m^2} \sqrt{\frac{Dt}{\pi}}, \quad (\text{D23})$$

and similarly, for the number of particles inside the channel,

$$\langle N_c^2(t) \rangle_{t \ll L_0^2/D} = 4 \frac{N}{L - L_0} \frac{\pi R^2}{4L_m^2} \sqrt{\frac{Dt}{\pi}}. \quad (\text{D24})$$

At intermediate times, corresponding to $L_0 q \rightarrow 0$ but $q/q_{\text{off}} \rightarrow \infty$, we obtain

$$\langle \Delta \hat{N}^2(s) \rangle = 4N \frac{\sqrt{D}}{s^{3/2}L} \frac{r}{L - L_0}, \quad (\text{D25})$$

yielding

$$\langle \Delta N^2(t) \rangle_{t \geq L_0^2/D} = 8 \frac{N}{L - L_0} \frac{\pi R^2}{4L_m^2} \sqrt{\frac{Dt}{\pi}}, \quad (\text{D26})$$

and similarly, for the number of particles inside the channel,

$$\langle N_c^2(t) \rangle_{t \geq L_0^2/D} = 8 \frac{N}{L-L_0} \frac{\pi R^2}{4L_m^2} \sqrt{\frac{Dt}{\pi}} \quad (\text{D27})$$

Going a bit further in time, we can investigate the infinite time limit for the number of particles, $q \rightarrow 0$. We obtain, as expected,

$$\langle \hat{N}_c^2(s) \rangle = 2N \frac{L_0}{sL} \frac{1}{1-L_0/L}, \quad (\text{D28})$$

yielding typically

$$\langle N_c^2(t) \rangle_{t \gg L_0^2/D} = 2N_0, \quad (\text{D29})$$

where N_0 is the mean number of particles inside the channel.

Coming back to the number difference at these intermediate times, taking now $q/q_{\text{off}} \rightarrow 0$ (but not too small),

$$\langle \Delta \hat{N}^2(s) \rangle = 4N \frac{\sqrt{D}}{s^{3/2}} \frac{r}{L-L_0} \frac{\sqrt{q_{\text{off}}/D}}{q} \quad (\text{D30})$$

such that we recover the intermediate, diffusive regime as

$$\langle \Delta N^2(t) \rangle_{t \geq q_{\text{off}}^{-1}} = 4 \frac{N}{L-L_0} \frac{\pi R^2}{4L_m^2} \sqrt{Dq_{\text{off}}t}, \quad (\text{D31})$$

and finally, at very long times ($q \rightarrow 0$),

$$\langle \Delta \hat{N}^2(s) \rangle = 4N \frac{\sqrt{D}}{s^{3/2}L} \frac{1}{1-L_0/L}, \quad (\text{D32})$$

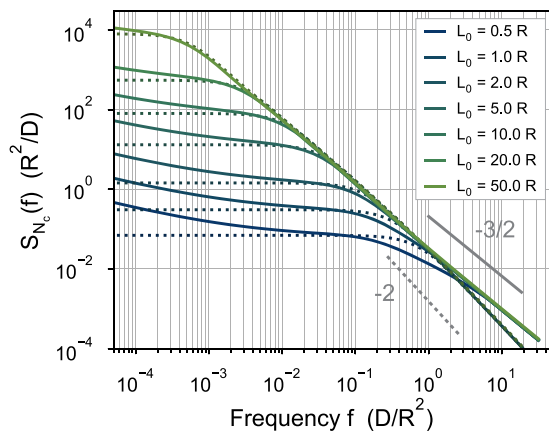


FIG. 13. Comparison of different methods: Fluctuation spectrum for the number of particles within the pore calculated using Eq. (60) (full line) and with Eq. (12) of Ref. 33 (dotted line). Here, we took $R = 0.2 L_m$ and $L = 500 R$. To compare with Eq. (12) of Ref. 33, we naturally used $D_b = D$ in their notations. Note that Eq. (12) had to be divided by a factor of 2 to show some degree of matching with our result Eq. (60).

yielding

$$\langle \Delta N^2(t) \rangle_{t \gg q_{\text{off}}^{-1}} = 8 \frac{N}{L-L_0} \sqrt{\frac{Dt}{\pi}}. \quad (\text{D33})$$

The emergence of all these limit regimes is shown in Figs. 11(b) and 12(b).

5. Comparison of the results with another method

In this paragraph, we compare the results of Eq. (60) with the results obtained with Eq. (12) of Ref. 33. Figure 13 shows the two solutions plotted for representative parameters. Disagreement between the two solutions is visible at low frequencies, at the frequency turning point, and at high frequencies where the decay exponent is not the same. Similar disagreement is found for other pore parameters.

DATA AVAILABILITY

The data that support the findings of this study are available from the corresponding author upon reasonable request.

REFERENCES

- S. M. Bezrukov and M. Winterhalter, "Examining noise sources at the single-molecule level: $1/f$ noise of an open maltoporin channel," *Phys. Rev. Lett.* **85**, 202 (2000).
- Z. Siwy and A. Fuliński, "Origin of $1/f$ noise in membrane channel currents," *Phys. Rev. Lett.* **89**, 158101 (2002).
- S. Marbach, D. S. Dean, and L. Bocquet, "Transport and dispersion across wiggling nanopores," *Nat. Phys.* **14**, 1108–1113 (2018).
- S. D. Lawley and C. E. Miles, "Diffusive search for diffusing targets with fluctuating diffusivity and gating," *J. Nonlinear Sci.* **29**, 2955–2985 (2019).
- L. Scalfi, D. T. Limmer, A. Coretti, S. Bonella, P. A. Madden, M. Salanne, and B. Rotenberg, "Charge fluctuations from molecular simulations in the constant-potential ensemble," *Phys. Chem. Chem. Phys.* **22**, 10480–10489 (2020).
- F. Wohnsland and R. Benz, " $1/f$ -noise of open bacterial porin channels," *J. Membr. Biol.* **158**, 77–85 (1997).
- E. M. Nestorovich, T. K. Rostovtseva, and S. M. Bezrukov, "Residue ionization and ion transport through OmpF channels," *Biophys. J.* **85**, 3718–3729 (2003).
- C. Dekker, "Solid-state nanopores," *Nat. Nanotechnol.* **2**, 209–215 (2007).
- R. M. M. Smeets, U. F. Keyser, N. H. Dekker, and C. Dekker, "Noise in solid-state nanopores," *Proc. Natl. Acad. Sci. U. S. A.* **105**, 417–421 (2008).
- R. M. M. Smeets, N. H. Dekker, and C. Dekker, "Low-frequency noise in solid-state nanopores," *Nanotechnology* **20**, 095501 (2009).
- M. R. Powell, I. Vlassiouk, C. Martens, and Z. S. Siwy, "Nonequilibrium $1/f$ noise in rectifying nanopores," *Phys. Rev. Lett.* **103**, 248104 (2009).
- D. P. Hoogerheide, S. Garaj, and J. A. Golovchenko, "Probing surface charge fluctuations with solid-state nanopores," *Phys. Rev. Lett.* **102**, 256804 (2009).
- C. Tasserit, A. Koutsioubas, D. Lairez, G. Zalcer, and M.-C. Clochard, "Pink noise of ionic conductance through single artificial nanopores revisited," *Phys. Rev. Lett.* **105**, 260602 (2010).
- M. R. Powell, N. Sa, M. Davenport, K. Healy, I. Vlassiouk, S. E. Létant, L. A. Baker, and Z. S. Siwy, "Noise properties of rectifying nanopores," *J. Phys. Chem. C* **115**, 8775–8783 (2011).
- S. J. Heerema, G. F. Schneider, M. Rozemuller, L. Vicarelli, H. W. Zandbergen, and C. Dekker, " $1/f$ noise in graphene nanopores," *Nanotechnology* **26**, 074001 (2015).
- E. Secchi, A. Niguès, L. Jubin, A. Siria, and L. Bocquet, "Scaling behavior for ionic transport and its fluctuations in individual carbon nanotubes," *Phys. Rev. Lett.* **116**, 154501 (2016).

- ¹⁷C. Wen, S. Zeng, K. Arstila, T. Sajavaara, Y. Zhu, Z. Zhang, and S.-L. Zhang, “Generalized noise study of solid-state nanopores at low frequencies,” *ACS Sens.* **2**, 300–307 (2017).
- ¹⁸A. Fragasso, S. Pud, and C. Dekker, “1/f noise in solid-state nanopores is governed by access and surface regions,” *Nanotechnology* **30**, 395202 (2019).
- ¹⁹S. F. Knowles, U. F. Keyser, and A. L. Thorneywork, “Noise properties of rectifying and non-rectifying nanopores,” *Nanotechnology* **31**, 10LT01 (2019).
- ²⁰M. A. G. Zevenbergen, D. Krapf, M. R. Zuddam, and S. G. Lemay, “Mesoscopic concentration fluctuations in a fluidic nanocavity detected by redox cycling,” *Nano Lett.* **7**, 384–388 (2007).
- ²¹M. A. G. Zevenbergen, P. S. Singh, E. D. Goluch, B. L. Wolfrum, and S. G. Lemay, “Stochastic sensing of single molecules in a nanofluidic electrochemical device,” *Nano Lett.* **11**, 2881–2886 (2011).
- ²²K. J. Krause, K. Mathwig, B. Wolfrum, and S. G. Lemay, “Brownian motion in electrochemical nanodevices,” *Eur. Phys. J. Spec. Top.* **223**, 3165–3178 (2014).
- ²³J. Clarke, H.-C. Wu, L. Jayasinghe, A. Patel, S. Reid, and H. Bayley, “Continuous base identification for single-molecule nanopore DNA sequencing,” *Nat. Nanotechnol.* **4**, 265–270 (2009).
- ²⁴S. Howorka and Z. Siwy, “Nanopore analytics: Sensing of single molecules,” *Chem. Soc. Rev.* **38**, 2360–2384 (2009).
- ²⁵S. W. Kowalczyk, A. R. Hall, and C. Dekker, “Detection of local protein structures along dna using solid-state nanopores,” *Nano Lett.* **10**, 324–328 (2010).
- ²⁶N. A. W. Bell and U. F. Keyser, “Specific protein detection using designed DNA carriers and nanopores,” *J. Am. Chem. Soc.* **137**, 2035–2041 (2015).
- ²⁷P. Chen, T. Mitsui, D. B. Farmer, J. Golovchenko, R. G. Gordon, and D. Branton, “Atomic layer deposition to fine-tune the surface properties and diameters of fabricated nanopores,” *Nano Lett.* **4**, 1333–1337 (2004).
- ²⁸V. Tabard-Cossa, D. Trivedi, M. Wiggan, N. N. Jetha, and A. Marziali, “Noise analysis and reduction in solid-state nanopores,” *Nanotechnology* **18**, 305505 (2007).
- ²⁹E. Beamish, H. Kwok, V. Tabard-Cossa, and M. Godin, “Precise control of the size and noise of solid-state nanopores using high electric fields,” *Nanotechnology* **23**, 405301 (2012).
- ³⁰A. Balan, B. Machielse, D. Niedzwiecki, J. Lin, P. Ong, R. Engelke, K. L. Shepard, and M. Drndić, “Improving signal-to-noise performance for DNA translocation in solid-state nanopores at MHz bandwidths,” *Nano Lett.* **14**, 7215–7220 (2014).
- ³¹H. Chang, F. Kosari, G. Andreadakis, M. A. Alam, G. Vasmatzis, and R. Bashir, “DNA-mediated fluctuations in ionic current through silicon oxide nanopore channels,” *Nano Lett.* **4**, 1551–1556 (2004).
- ³²S. F. Knowles, N. E. Weckman, V. J. Lim, D. J. Bonthuis, U. F. Keyser, and A. L. Thorneywork, “Investigating noise signatures of polymer adsorption using nanopores,” [arXiv:2012.00884](https://arxiv.org/abs/2012.00884) (2020).
- ³³S. M. Bezrukavov, A. M. Berezhkovskii, M. A. Pustovoit, and A. Szabo, “Particle number fluctuations in a membrane channel,” *J. Chem. Phys.* **113**, 8206–8211 (2000).
- ³⁴M. Zorkot and R. Golestanian, “Current fluctuations across a nano-pore,” *J. Phys.: Condens. Matter* **30**, 134001 (2018).
- ³⁵S. Gravelle, R. R. Netz, and L. Bocquet, “Adsorption kinetics in open nanopores as a source of low-frequency noise,” *Nano Lett.* **19**, 7265–7272 (2019).
- ³⁶M. Zorkot, R. Golestanian, and D. J. Bonthuis, “Current fluctuations in nanopores: The effects of electrostatic and hydrodynamic interactions,” *Eur. Phys. J. Spec. Top.* **225**, 1583–1594 (2016).
- ³⁷M. Zorkot, R. Golestanian, and D. J. Bonthuis, “The power spectrum of ionic nanopore currents: The role of ion correlations,” *Nano Lett.* **16**, 2205–2212 (2016).
- ³⁸S. Marbach and L. Bocquet, “Osmosis, from molecular insights to large-scale applications,” *Chem. Soc. Rev.* **48**, 3102–3144 (2019).
- ³⁹T. E. Harris, “Diffusion with collisions between particles,” *J. Appl. Probab.* **2**, 323–338 (1965).
- ⁴⁰D. Dürr, S. Goldstein, and J. L. Lebowitz, “Asymptotics of particle trajectories in infinite one-dimensional systems with collisions,” *Commun. Pure Appl. Math.* **38**, 573–597 (1985).
- ⁴¹M. A. G. Zevenbergen, P. S. Singh, E. D. Goluch, B. L. Wolfrum, and S. G. Lemay, “Electrochemical correlation spectroscopy in nanofluidic cavities,” *Anal. Chem.* **81**, 8203–8212 (2009).
- ⁴²J. Crank, *The Mathematics of Diffusion* (Oxford University Press, 1979).
- ⁴³B. B. Mandelbrot and J. W. Van Ness, “Fractional Brownian motions, fractional noises and applications,” *SIAM Rev.* **10**, 422–437 (1968).
- ⁴⁴S. Burov, J.-H. Jeon, R. Metzler, and E. Barkai, “Single particle tracking in systems showing anomalous diffusion: The role of weak ergodicity breaking,” *Phys. Chem. Chem. Phys.* **13**, 1800–1812 (2011).
- ⁴⁵D. Krapf, N. Lukat, E. Marinari, R. Metzler, G. Oshanin, C. Selhuber-Unkel, A. Squarcini, L. Stadler, M. Weiss, and X. Xu, “Spectral content of a single non-Brownian trajectory,” *Phys. Rev. X* **9**, 011019 (2019).
- ⁴⁶L. Bocquet and E. Charlaix, “Nanofluidics, from bulk to interfaces,” *Chem. Soc. Rev.* **39**, 1073–1095 (2010).
- ⁴⁷D. Yilmaz, D. Kaya, K. Kececi, and A. Dinler, “Role of nanopore geometry in particle resolution by resistive-pulse sensing,” *ChemistrySelect* **6**, 59–67 (2021).
- ⁴⁸G. G. MacFarlane, “A theory of contact noise in semiconductors,” *Proc. Phys. Soc., Sect. B* **63**, 807 (1950).
- ⁴⁹K. Van Vliet and J. Fassett, *Fluctuation Phenomena in Solids* (Academic Press: New York, 1965), Chap. 7.
- ⁵⁰W. Deng and E. Barkai, “Ergodic properties of fractional Brownian-Langevin motion,” *Phys. Rev. E* **79**, 011112 (2009).
- ⁵¹S. M. A. Tabei, S. Burov, H. Y. Kim, A. Kuznetsov, T. Huynh, J. Jureller, L. H. Philipson, A. R. Dinner, and N. F. Scherer, “Intracellular transport of insulin granules is a subordinated random walk,” *Proc. Natl. Acad. Sci. U. S. A.* **110**, 4911–4916 (2013).
- ⁵²A. D. Fernández, P. Charchar, A. G. Cherstvy, R. Metzler, and M. W. Finnis, “The diffusion of doxorubicin drug molecules in silica nanoslits is non-Gaussian, intermittent and anticorrelated,” *Phys. Chem. Chem. Phys.* **22**, 27955 (2020).
- ⁵³O. Rauh, U.-P. Hansen, S. Mach, A. J. W. Hartel, K. L. Shepard, G. Thiel, and I. Schroeder, “Extended beta distributions open the access to fast gating in bilayer experiments—Assigning the voltage-dependent gating to the selectivity filter,” *FEBS Lett.* **591**, 3850–3860 (2017).
- ⁵⁴D. Lesnicki, C. Y. Gao, B. Rotenberg, and D. T. Limmer, “Field-dependent ionic conductivities from generalized fluctuation-dissipation relations,” *Phys. Rev. Lett.* **124**, 206001 (2020).
- ⁵⁵A. Scala, T. Voigtmann, and C. De Michele, “Event-driven Brownian dynamics for hard spheres,” *J. Chem. Phys.* **126**, 134109 (2007).